Agreement INGV-DPC 2007-2009

Project S4: ITALIAN STRONG MOTION DATA BASE

Responsibles: Francesca Pacor, INGV Milano – Pavia
and Roberto Paolucci, Politecnico Milano

http://esse4.mi.ingv.it

Deliverable # 7

APPLICATION OF SURFACE-WAVES METHODS FOR SEISMIC SITE CHARACTERIZATION OF ITACA STATIONS

Appendix

June 2010

edited by:

UR4 Sebastiano Foti, Politecnico di Torino

UR8 Stefano Parolai, Helmholtz Centre Potsdam GFZ German Research Centre for Geosciences

UR7 Dario Albarello, Università di Siena

Contributors

UR1 – INGV Milano

Rodolfo Puglia

UR2 – INGV Roma

Giuliano Milana, Giuseppe Di Giulio, Fabrizio Cara, Paola Bordoni, Riccardo Azzara, Francesco Bergamaschi

UR4 – Politecnico di Torino

Paolo Bergamo, Cesare Comina (Università di Torino), Sebastiano Foti, Margherita Maraschini, Ken Tokeshi

UR7 – Università di Siena

Dario Albarello, Enrico Lunedei, Domenico Pileggi, David Rossi

UR8 – Helmholtz Centre Potsdam GFZ German Research Centre for Geosciences

Stefano Parolai, Matteo Picozzi

Table of Contents

1. Introduction

This paper reports of surface wave tests carried out at selected sites of the Italian accelerometric stations (RAN) for the estimation of the subsoil S-wave velocity. The shear wave velocity model estimated allows both a classification of the accelerometric station following the existing normative and the evaluation of new proxies for site effects (see Deliverable D13). Surface wave analysis has been chosen as the primary investigation method since it offers the possibility of reaching the required accuracy at reasonable costs.

Several RUs have contributed to this task. The use of different surface wave methods allows the different geological situations (thin/thick deposits, profiles with large impedance contrasts etc..) to be investigated.

From the shear wave velocity model estimated some relevant parameters for the site classification, such as Vs30, the seismic bedrock depth (conventionally defined as the interface below whom Vs>800 m/s, according to EC8), the average Vs to the seismic bedrock and the natural frequency in case of shallow seismic bedrock site, can be estimated.

In Chapter 2 criteria for the selection of RAN stations to be characterised and of methods to be applied are summarized. A map with the location of the sites that were investigated is shown. Chapter 3 describes the techniques used by the different RUs. After a short introduction of surface wave methods, acquisition setup and inversion methods are described for each Research Unit. In Chapter 4 some examples of the analysis performed by the RUs are reported, in order to highlight the different methodologies used. Finally, in Chapter 5, a table is reported to summarize the results of all the RUs.

2. Investigated sites

2.1. Criteria for selection

The selection of RAN sites to be characterized with surface wave analysis was driven by several criteria. First, as a general criterion, the attention was pointed to stations that recorded interesting events in the past and to the recently installed digital stations. Moreover, it was paid attention to have a good coverage for the whole Italian territory, excluding regions with a higher availability of results from previous surveys. Furthermore, due to the occurrence of the strong L'Aquila earthquake on April 2009, priority was attributed to RAN station located in area interested by this event.

In general, priority was attributed to sites where surface waves techniques could be applied more effectively. In particular, on the basis of a preliminary analysis of the ITACA station monographies and with the help of Google Earth imagines analysis, sites with complicated topography and with no sufficient space for carrying out the surface wave measurements were excluded. However, a sub set of sites to be analysed were also selected just to check the feasibility of surface waves techniques in "difficult sites" (e.g., rock/stiff soil sites with rugged topography).

The large set of sites selected in this preliminary phase was then inspected through field investigations that allowed a nearly-final list of selected sites to be defined. The preliminary field investigations were meant at verifying the suitability of the sites for surface wave method investigation.

Considering the geological characteristics of the selected sites (thin, i.e. meters/tens of meters of soft sediments, or thick, i.e. hundreds of meters of soft sediments, rock/stiff soil configurations) it was decided to assign them amongst the different UR involved in the work package by considering their expertise. In particular, it was decided that thin sedimentary covers sites were assigned mainly to UR with large experience in active methods and with appropriate instruments (multi-channel acquisition systems with high frequency geophones) while the deep basins and rock/stiff soil configurations were assigned to the URs with large experience in passive source methods and equipped with short period seismometers.

Considering the target of the survey, different strategies were used. For example at sites with very shallow seismic bedrock (as for example in Liguria and in the south-east of Sicily, where only thin rock alteration zone are present close to the ground surface waves) only active surface wave tests with multistation testing setup (MASW) were used. At site with very deep seismic bedrock, as for example in the Po Plain, only passive methods with 2D arrays were used. In intermediate situations, a combination of active and passive methods was to guarantee adequate depth of exploration and good resolution at shallow depth. Moreover, selected rock sites were thoroughly investigated to assess the effects of faulting, jointing and weathering with a combination of surface wave surveys and classical geomechanical approaches. In this case, detailed geological surveys carried on at the scale 1:5000 revealed to be of great importance.

The ultimate list of the investigated sites was obtained after the field measurement campaign since some changes were necessary because of logistic problems.

A map of the investigated sites is shown in Figure 1.

Figure 1 Map of the investigated sites

3. Details on the techniques

In this section there is a summary on the techniques used for the site characterization. After a short introduction of surface wave method, each RU describes the acquisition, processing and inversion method used for the determination of the soil model.

3.1. Surface wave methods

Surface wave methods (S.W.M.) are based on the geometrical dispersion, which makes Rayleigh wave velocity frequency dependent in vertically heterogeneous media. High frequency (short wavelength) Rayleigh waves propagate in shallow zones close to the free surface and are informative about their mechanical properties, whereas low frequency (long wavelength) components involve deeper layers. Surface wave tests are typically devoted to the determination of a small strain stiffness profile for the site under investigation. Consequently the dispersion curve will be associated to the variation of medium parameters with depth.

The calculation of the dispersion curve from model parameters is the so called forward problem. Surface wave propagation can be seen as the combination of multiple modes of propagation, i.e. more than one possible velocity can be associated to each frequency value. Including higher modes in the inversion process allows the penetration depth to be increased and a more accurate subsoil profile to be retrieved.

If the dispersion curve is estimated on the basis of experimental data, it is then possible to solve the inverse problem, i.e. the model parameters are identified on the basis of the experimental data collected on the boundary of the medium. The result of the surface wave method is a one-dimensional S wave velocity soil profile.

The standard procedure for surface wave tests is reported in Figure 2. It can be subdivided into three main steps:

- acquisition of experimental data;
- signal processing to obtain the experimental dispersion curve;
- inversion process to estimate shear wave velocity profile at the site.

It is very important to recognize that the above steps are strongly interconnected and their interaction must be adequately accounted for during the whole interpretation process.

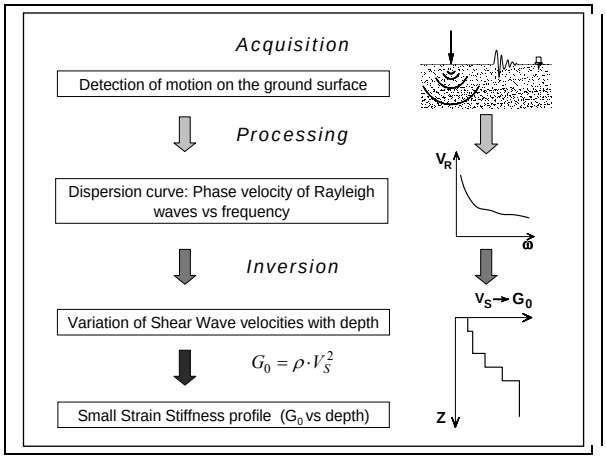

Figure 2– Flow chart of surface wave analysis.

The primary use of surface wave testing is related to site characterization in terms of shear wave velocity profile. The V_S profile is of primary interest for seismic site response studies and for studies of vibration of foundations and vibration transmission in soils. Other applications are related to the prediction of settlements and to soil-structure interaction.

With respect to the evaluation of seismic site response, it is worth noting the affinity between the model used for the interpretation of surface wave tests and the model adopted for most site responses study. Indeed the application of equivalent linear elastic methods is often associated with layered models (e.g. the code SHAKE and all similar approaches). This affinity is also particularly important in the light of equivalence problems, which arise because of non-uniqueness of the solution in inverse problems. Indeed profiles which are equivalent in terms of Rayleigh wave propagation are also equivalent in term of seismic amplification (Foti et al., 2009).

Many seismic building codes introduce the weighted average of the shear wave velocity profile in the shallowest 30m as to discriminate class of soils to which a similar site amplification effect can be associated. The so-called $V_{S,30}$ can be evaluated very efficiently with surface wave method also because its average nature does not require the high level of accuracy that can be obtained with seismic borehole methods (such as Cross-Hole tests and Down-Hole tests). Comina et al. (2010) studied the accuracy and reliability of surface wave tests for the evaluation of $V_{S,30}$, showing that uncertainties on single model parameters are much higher of uncertainties on integral parameters such as $V_{S,30}$ (see for example Figure 3).

A detailed description on the different methods is given in Deliverable #6. Acquisition, processing and inversion methods of each RU are summarized in the following paragraphs.

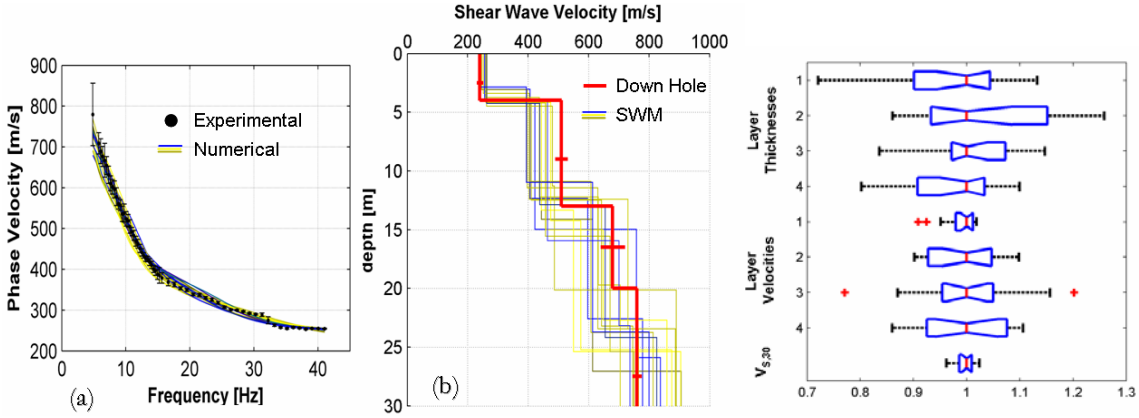

Figure 3 – Uncertainties associated to solution non-uniqueness in surface wave analysis: a) experimental and numerical dispersion curves; b) best fitting VS profiles; c) normalised uncertainties on single model parameters and on VS,30 (Comina et al., 2010)

3.2. UR2 – INGV Roma

The UR used two different types of equipment according to the array layout (1D versus 2D geometry).

For 1D arrays, the data were collected by three Geometrics-GEODE data loggers connected in a LAN configuration. The GEODE is a 24 channels instrument based on a 24 bits AD converter. The data acquisition is driven by a laptop PC that is also used as data storage unit. Data are stored in SEG2 binary format. The maximum number of available channels is 72 with a maximum geophones spacing of 10 meters. The sensors connected to the GEODE's line are GEOSPACE vertical geophones with a natural frequency of 4.5 Hz. 1D array is used both for active and passive data acquisition. A minigun source is used for active surveys.

For 2D arrays we used 12 or 13 stand alone seismic instruments based on Reftek 130 (24 bits) and Lennartz Marslite (21 bits) data loggers. Each unit, synchronized using GPS receivers, operated in continuous recording mode with a sampling rate of 200-250 samples per second. Data were recorded in a native binary format and converted in SEGY or SEG2 format. The recording units were connected to Lennartz LE3D-5s seismometers with a natural frequency of 0.2 Hz and high sensitivity (400 V/m/s). This choice allows exploring the low resonance frequencies expected for sites located on deep alluvial planes. To reduce the bias introduced by errors in sensors location, the position of the stations is determined by differential GPS measurements obtained performing a real time kinematic survey with a Leica Systems 1200 GNSS instrument. The differential corrections are obtained through a GPRS connection to a network of reference stations (www.italpos.it). The positioning system consents to operate in real time providing distance and azimuth between any couple of points in the array. This feature allows to draw the array's geometry in advance and to easily find the position of the recording stations on the field. With this approach the error in positioning can be lowered to few (5-10) centimetres.

The 1D array typical acquisition scheme is based on 72 geophones with a spacing distance chosen according to the desired depth of investigation. For shallow seismic bedrock the spacing was set to 1 meter for a total deployment length of 71 meters. Only in one case (Cassino R.AN. station CSS), due to the lack of space, we deployed 54 sensors for a total length of 53 meters. For deeper sites geophones spacing was set to 2 meters for a deployment length of 142 meters. For the site of Dicomano both 1 and 2 meters spacing geometry was adopted. Before data acquisition, the quality of signals was controlled by the noise monitor utility that allows checking the right sequence of geophones on the line and their coupling with the ground. For every deployment the minigun source was set at both sides of the array with an offset ranging from 40 to 0 meters. For each side of the array two separate offsets were selected. For every offset at least two shots were performed. Two extra shots were located just at the centre of the deployment. The symmetry in shots layout allows verifying the one-dimensional behaviour of the investigated site as required by the MASW technique. Sampling rate was set at 0.125 ms with a record duration of 2 seconds (16000 points). For passive data acquisition the geometry was not changed, the sampling rate was set to 2 ms with a record length of 30 seconds (16000) points. At least 10 time windows were recorded in this case. Wherever possible we also used a heavy vehicle moving close to the end of deployment as noise source. In this case we used the acquisition scheme used for passive 1D data.

The geometry of 2D arrays depends on the investigation depth. Deeper sites require array with a wider aperture. The use of 2D arrays and passive technique consents to investigate frequencies lower than those detected by active survey. The general array layout is based on a central station surrounded by three outer rings formed by a number of stations ranging from 3 and 5. The distance between the centre and the rings ranges from 10 to 200-300 meters and allows tuning the response of the array in the desired frequency range. The geometry of 2D array is designed in order to obtain a full azimuthal coverage. A preliminary analysis of the theoretical array response can suggest the frequency range detected by the chosen geometry. The use of remote stations gives a high flexibility in the array deployment and allows to easily adjusting according to the morphology and to the logistic of the site. Figure 4 shows the geometry of the array installed at Assergi (R.A.N. station GSA). For the other sites the geometry was basically the same with a different array aperture.

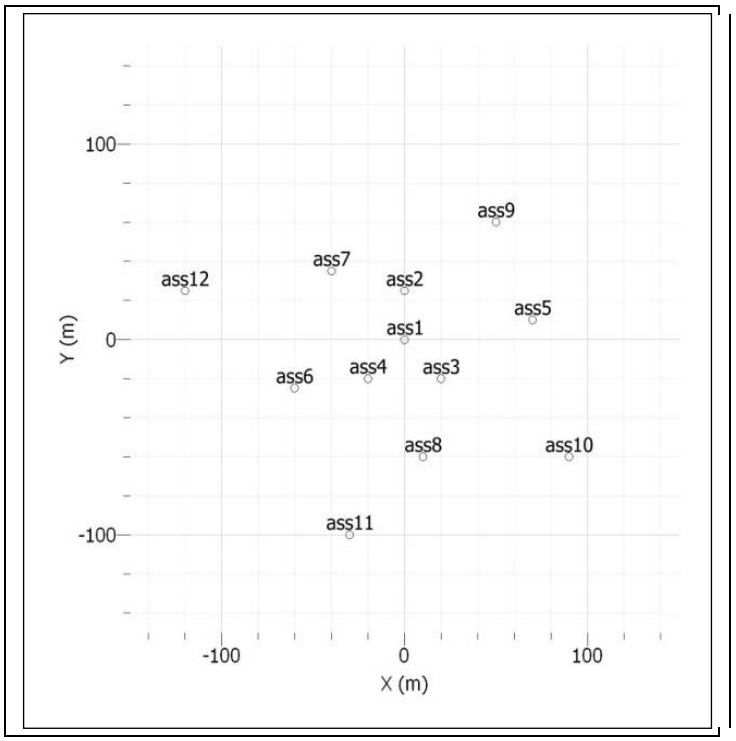

Figure 4 – 2D array layout for the Assergi site. The ass6 station corresponds to the RAN site GSA.

The 2D arrays recorded long time windows of seismic noise. The typical duration of acquisition was between 1 and 2 hours.

The 2D array stations can also be used for HVNSR analysis aimed to identify the resonance frequency of the sites. Microtremor data are also useful to study the spatial stability of H/V ratios and to identify the presence of lateral variation in the geology of the sites. For the sites where only 1D array were deployed we performed anyway microtremor measurements using a single station.

Data were processed in order to find the experimental dispersion curve for Rayleigh waves. For 1D array data, three different computer codes were used: Optim R.e.m.i (Louie, 2001), Geopsy (www.geopsy.org) and an original INGV software. For 2D array data only the Geopsy software was utilized.

The approach used in Remi is based on the velocity spectral analysis called the □-p transformation, or the Slant Stack transform, described by Thorson and Claerbout (1985). This transformation takes a record section of multiple seismograms, with seismogram amplitudes relative to distance and time (x-t), and converts it to amplitudes relative to the ray parameter p (the inverse of apparent velocity) and an intercept time tau. It is familiar to array analysts as ``beam forming,'' and has similar objectives to a two-dimensional Fourier-spectrum or ``F-K'' analysis as described by Horike (1985). The other two codes are both based on Frequency Wavenumber (FK) analysis, both conventional and high resolution. The basic idea of f-k processing consists of delaying the observed recordings at different stations according to a particular horizontal wavenumber vector and computing the semblance coefficient or coherence measure (see Neiddell and Taner (1971), Douze and Laster (1979)) and/or beam power of the shifted stacked output of all array stations. The high resolution frequency wavenumber (hrfk) algorithm follows the ideas of Capon (1969). It can be viewed as a generalized beamforming algorithm resulting in an auto-adaptive (optimal) complex spatial weighting scheme. For analysis of narrowband stationary signals, it is one of the most common and preferred frequency wavenumber techniques applied to ambient vibration

analysis. An extra tool for passive 2D array analysis is given by the Modified Spatial Autocorrelation (MSPAC) introduced by Bettig et al. (2001). This technique represents a generalization of the original approach by Aki (1957) based on spatial autocorrelation of noise time windows and its link to Bessel functions whose depends on frequency, distance and wave velocity.

For active data the analysis is performed in a short time window that contains the energy related to the seismic source. For passive data the analysis (both 1D and 2D) is performed on a short moving window on the entire signal in order to obtain for each frequency and for each window a value of phase velocity. In this case the use of multiple windows allows to perform a statistical analysis on the results and to derive an uncertainty value for the dispersion curve.

All the codes we used are installed on the laptop computer operating on the field. This allows a rapid evaluation of the dispersion curve in order to quickly control the quality of the data. The preliminary check on recorded data can suggest some adjustment on the array geometry in order to improve the quality of recorded signals.

For the inversion of the dispersion curve we use the Neighbourhood Algorithm (Sambridge, 1999) as implemented by Wathelet (2008) in order to invert the experimental curves (*www.geopsy.org*). Neighbourhood Algorithm is a directed-search method for nonlinear inversion making use of Voronoi cells to investigate the multidimensional model space and to generate iteratively new random models inside the most promising cells. The tuning parameters are ni, ns and nr. A misfit function is first computed for the initial set of ni models. Within the nr cells with the lowest misfit a total of ns new models are added (ns/nr samples generated per cell). The last two steps are repeated N times resulting in a total of ni + N*ns models. We stop the inversion when the plateau-branch of the misfit trend was reached.

We considered distinct parameterization classes of the model space to invert the surface-wave dispersion, i.e. we used models with constant velocity inside layers or models with increasing velocity in the single layers. This velocity increase can be both linear and exponential. Inside each layer the free parameters are Vs, the ratio Vs/Vp and the thickness. However, the most important parameter in surface wave inversion is Vs. In each layer, we link the Vp interface to the Vs interface. We typically allow for each layer a Vs range from 50 to 2500 m/s that was increased to 150-3500 m/s for the halfspace. The compressional velocity (Vp) varies from 200 to 5000 m/s with the Poisson's Ratio uniform in the range 0.2-0.5. We fix the density to 2 t/m3 consistently with its low influence on surface wave dispersion. In the inversion scheme it is possible to take into account the contribution of both fundamental and higher modes of Rayleigh waves.
The misfit measure (m) between observed and theoretical dispersion curves is computed for each inverted model and is defined as:

$$m=\sqrt{\sum_{i=0}^{n_f}\frac{(x_{di}-x_{ci})^2}{\sigma_i^2\cdot n_f}}$$

where x_{di} and x_{ci} are the phase-velocity of observed and theoretical dispersion curve at frequency f_i, respectively. σi is the uncertainty of the datum at frequency i and nf is the total number of samples. For sake of simplicity we do not allow the presence of low velocity zones (LVZ) during the inversion process.

3.3. UR4 – Politecnico di Torino

3.3.1. Acquisition

In all the considered sites MASW tests were performed. The acquisition geometry used for MASW tests was also used to perform refraction measurements. In some stations also passive tests were performed.
Characteristics of sensors for active and passive measurements are reported in Table 1. An example of acquisition geometry is shown in Figure 5. The source for active tests was a 5 kg sledgehammer hitting either a Teflon or a metal plate.

Test	GEOPHONE TYPE	NATURAL FREQUENCY	GEOPHONE NUMBER
MASW/ Refraction	vertical SENSOR SM-6/U-B	4,5 Hz	from 24 to 48
Passive surface wave tests	three components 3D HS1 GEO-SPACE	2 Hz	4
	vertical HS1 GEO-SPACE	2 Hz	12

Table 1 receiver characteristics

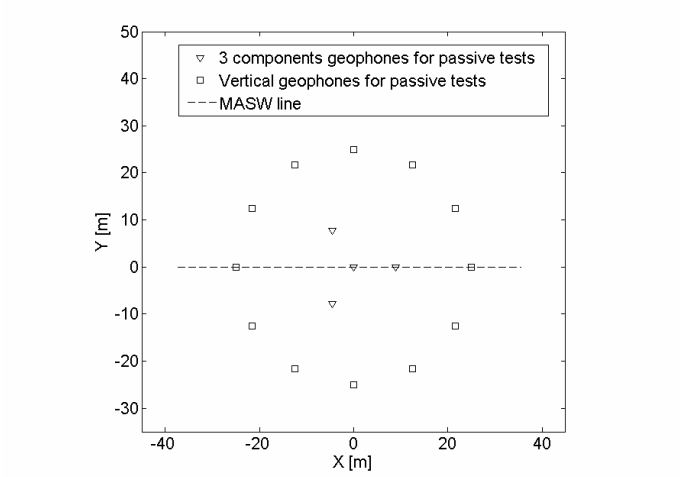

Figure 5 – Example of acquisition geometry.

3.3.2. Processing of active surface wave data

The processing allows the experimental dispersion curve to be determined.

Multichannel data are processed using a double Fourier Transform, which generates the frequency-wave number spectrum, where the multimodal dispersion curve is easily extracted as the location of spectral maxima.

3.3.3. Processing of passive surface wave data

The phase velocity of the surface waves can be extracted from noise recordings by using different methods: among them, the most frequently used are the Beam-Forming Method (BFM) (Lacoss et al., 1969) and the Maximum Likelihood Method (MLM) (Capon, 1969). Here we will illustrate the Beam-Forming Method which was used to process passive surface wave data.

The estimate of the F-K spectra $P_b(f,\mathrm{k})$ by the BFM is given by:

$$P_b(f,k) = \sum_{l,m=1}^{n} \phi_{lm} \exp\{ik(X_l - X_m\} \ ,$$

where f is the frequency, k the two-dimensional horizontal wavenumber vector, n the number of sensors, ϕ_{lm} the estimate of the cross-power spectra between the l^{th} and the m^{th} data, and X_i and X_m, are the coordinates of the l^{th} and m^{th} sensors, respectively.

From the peak in the F-K spectrum occurring at coordinates k_{xo} and k_{yo} for a certain frequency f_0, the phase velocity c_0 can be calculated by:

$$c_0 = \frac{2\pi f_0}{\sqrt{k_{xo}^{\ 2} + k_{yo}^{\ 2}}}$$

so that, again, an experimental dispersion curve is retrieved.

Figure 6 shows an example of F-K analysis results obtained by processing passive surface wave data with Beam-Forming Method: white dots indicate the position of the maximum used to estimate the phase velocity while the white circle joins points with the same k values.

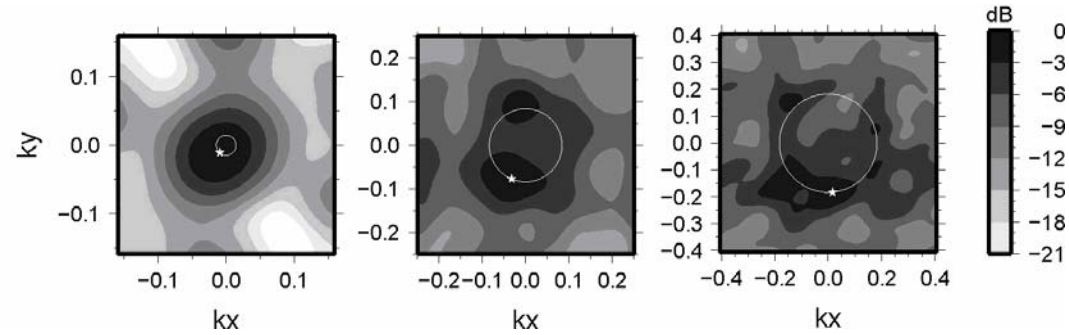

Figure 6 – Example of results from F-K analysis s for 2.5 Hz, 3.9 Hz, and 6.5 Hz. White dots indicate the position of the maximum used to estimate the phase velocity. The white circle joins points with the same k

3.3.4. Inversion of surface waves

The solution of the inverse Rayleigh problem is the final step in test interpretation. The solution of the forward problem forms the basis of any inversion strategy; the forward problem consists in the calculation of the function whose zeros are dispersion curves of a given model. Assuming a model for the soil deposit, model parameters of the best fitting subsoil profile are obtained minimizing an object function.

The subsoil is modelled as a horizontally layered medium overlaying a halfspace, with constant parameter in the interior of each layer and linear elastic behaviour. Model parameters are thickness, S-wave velocity, P-wave velocity (or Poisson coefficient), and density of each layer and the halfspace. The inversion is performed on S-wave velocities and thicknesses, whereas for the other parameters realistic values are chosen a priori. The number of layer is chosen applying minimum parameterization criterion.

In surface wave analysis it is very common to perform the inversions using only the fundamental mode of propagation. This approach is based on the assumption that the prevailing mode of propagation is the fundamental one; if this is partially true for normal dispersive sites, in several real cases the experimental dispersion curve is on the contrary the result of the superposition of several modes (Maraschini et al, 2010). This may happen in particular when velocity inversions or strong velocity contrasts are present in the shear wave velocity profile. In these stratigraphic conditions the inversion of the only fundamental mode will produce significant errors; moreover all the information contained in higher propagating

modes is not used in the inversion process. Therefore, the fundamental mode inversion does not use all the available information, and this affects the result accuracy.

The use of higher modes in the inversion can be helpful both in the low frequency range, in order to increase the investigation depth and to avoid the overestimation of the seismic bedrock velocity, and in the high frequency range in order to provide a more consistent interpretation of shallow interfaces and increase model parameter resolution.

In this work a multimodal misfit function has been used. This function is based on the Haskell-Thomson method for dispersion curve calculation (Thomson 1950, Haskell 1953, Herrmann e Wang 1980, Herrmann 2002). For a given subsoil model, and an experimental data, the misfit of the model is the L^1 norm of the vector containing the absolute value of the determinant of the Haskell-Thomson matrix (which is zeros in correspondence of all the modes of the dispersion curves of the numerical model) evaluated in correspondence of the experimental data (Maraschini et al. 2010). The misfit function adopted has the advantage of being able to include any dispersive event present in the data without the need of specifying to which mode the data points belong to, avoiding errors arising from mode misidentification, in particular in the low frequency range (Figure 8).

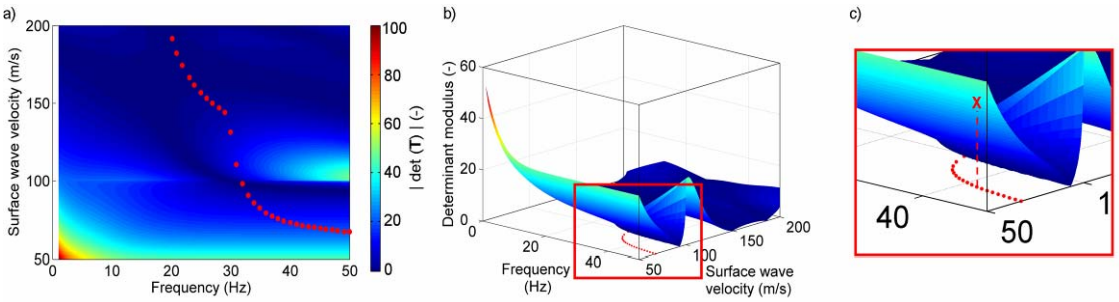

Figure 7 – Determinant misfit calculation: red points represent the experimental dispersion curve points, and the surface represent the absolute value of the determinant of the Haskell-Thomson matrix of a trial model. a) 2D view; b) 3D view; c) zoom of 3D view. The vertical segment represents the misfit associated to a given point of the experimental dispersion curve.

This misfit function is applied in a Global Search Method (Maraschini and Foti, 2010), in order to reduce the possibility of falling in local minima. A uniform random search is applied; ranges for the inversion have been chosen, for the different sites, based on the experimental dispersion curves; in particular the range of the S-wave half space velocity is close to the maximum surface wave velocity retrieved on experimental data.

The results of the inversion are reported as the ensemble of the best shear wave velocity profiles chosen according to a chi-square test (see Socco et al., 2008). It can be assumed that the experimental dispersion curve is affected by a Gaussian error with a known standard deviation, so that the probability density function of data $\rho D(d)$ can be described by a discrete m-dimensional Gaussian and the sample variance variable of each random vector (dispersion curve) extracted from the data pdf is distributed according to a chi-square probability density. According to these assumptions we adopt a misfit function with the structure of a chi-square and this allows a statistical test to be applied to the variances of the synthetic dispersion curves with respect to the experimental one dobs. Assuming that the best fitting curve dopt belongs to the distribution $\rho D(dobs)$ all models belonging to the distribution $\rho D(dopt)$ and consistent with the data within a fixed level of confidence α are selected. As the ratio between chi-square variables follows a Fisher distribution a one–tailed F test can be performed:

$$F_{\alpha}(dof_{dopt}, dof_{g(m)}) < \frac{\chi^2_{dopt}}{\chi^2_{g(m)}}$$

where α is the chosen level of confidence, dof_{dopt} and $dof_{g(m)}$ are the degrees of freedom of the Fischer distribution and χ^2_{dopt} and $\chi^2_{g(m)}$ are the misfit of the best fitting curve and the misfit of all the others respectively. All models passing such test are selected. In the figures reported a representation based on the misfit is adopted for velocity profiles, so that the darkest colour corresponds to the profile whose dispersion curve has the lowest misfit and better approximation to the reference one; instead for dispersion curves the coloured surface under imposed to the experimental one is a misfit surface, whose zeros are synthetic dispersion curve of the best fitting model.

The numerical codes used for processing and inversion of surface waves are non commercial codes, implemented at Politecnico di Torino.

3.4. UR8 – Helmholtz Centre Potsdam GFZ

RU8 focused on the characterization of sites with sedimentary cover thickness larger than 30 meters. For this purpose, the RU8 carried out 2D array measurements on 12 sites, 11 of which corresponding to sites where accelerometric stations of the RAN are located (Figure 1**,** Table 2). Moreover, following the L'Aquila (Italy) seismic sequence, 2009, a 2D array was carried out in the village of Onna (AQ) – nearby a seismic station of a temporary network installed in the framework of a cooperation between the INGV and other International Institutes, that recorded several aftershocks –, aiming to obtain the necessary information for the microzonation of the site.

Code	Site	Latitude	Longitude	# of stat.	hours.min
BVG	BEVAGNA	42.932	12.611	15	3.20
NRZI	NORCIA Z. I.	42.779	13.101	14	3.40
GRM	GRUMENTO NOVA	40.314	15.887	15	3.00
SNA	SANT ARCANGELO	40.258	16.249	13	1.40
LGN	LAGONEGRO	40.130	15.760	15	1.00
BZZ	BAZZANO	42.201	13.281	17	2.00
MI03	ONNA	42.194	13.284	17	3.00
CTL	CATTOLICA	43.952	12.736	14	2.00
ARG	ARGENTA	44.625	11.822	16	2.00
FAZ	FAENZA	44.293	11.888	16	4.00
MDN	MODENA	44.642	10.887	17	1.30
NVL	NOVELLARA	44.839	10.725	17	2.30

Table 2 RU8 array measurements.

3.4.1. Testing equipment

The arrays measurements carried out by the RU8 were performed using between 13 and 17 EDL 24bit acquisition systems equipped with short-period Mark-L4-C-3D 1Hz sensors and GPS timing. The unique exception was BVG, where 15 LE-3D/5s sensors coupled with Reftek 130 digitizers (24bit) were adopted. In this case, measurements were carried out by INGV-Mi in September 2007.

3.4.2. Typical testing layouts

Microtremor measurements in 2D array configuration were carried out using sensors inter-distances between 5 m and about 250 m (Figure 8). The stations worked contemporary for more than 1 hour (Table 2), recording noise at 200 s.p.s. (only at BVG 500 s.p.s. was used), which is adequate for the short inter-station distance considered. Sensors were installed so as to obtain a good coupling between the instrument and soil, and where possible, avoiding asphalt. Moreover sensors were covered in order to reduce any interference caused by wind.

3.4.3. Processing

For each site, the Rayleigh wave dispersion curve was estimated by analysing the vertical component of the recorded microtremors. In particular, the Extended Spatial Auto Correlation (ESAC; Ohori et al., 2002; Deliverable 6, 2009) and the Frequency-Wavenumber (FK; Lacoss et al., 1969; Deliverable 6, 2009) methods were adopted. The analyses were carried out using between 30 and 240 non-overlapping signal windows.

The Horizontal-to-Vertical (H/V) spectral ratio curves were computed (Deliverable 6, 2009) for each station of the arrays, using the three component ground motion microtremor recordings, and between 60 and 240 non-overlapping signal windows. In particular, each window 60 seconds long was tapered with a 5 per cent cosine function before the computation of the spectra. Then, the Fourier spectra were computed for each noise component and smoothed using: a Hanning window of 10% relative bandwidth for MI03 and BZZ records. A Konno and Ohmachi (1998) window (with b=40) was used for the other arrays. This ensures the reduction of numerical instabilities while preserving the major features of the spectra, especially the flanks of the *H/V* ratios maxima. The resulting spectral ordinates relative to horizontal components were geometrically averaged and divided by the vertical spectral ordinate to compute the *H/V* function.

3.4.4. Inversion algorithm

For the sites where both high-quality Rayleigh wave dispersion and *H/V* ratio curves were derived, a joint inversion scheme, as that proposed by Parolai et al. 2005 and 2006, was used to estimate the local S-wave velocity profile.

In particular, the non-linear inversions were performed using a genetic algorithm, which does not rely upon an explicit starting model and allows the identification of the solution close to the global minimum. Here, the genetic algorithm proposed by Yamanaka and Ishida (1996) was used. The forward modelling of Rayleigh wave phase velocities and *H/V* curves was performed using the modified Thomson-Haskell method proposed by Wang (1999) and following the suggestions of Tokimatsu et al. (1992) and Arai and Tokimatsu (2004), under the assumption of vertically heterogeneous 1D earth models. The validity of this assumption is investigated by computing the *H/V* curve for each station of the array. Whenever the *H/V* curves provide the same estimate of the fundamental frequency and the main peak exhibits a good level of shape similarity, it is reasonable to assume that the geological structure

underneath the array does not change significantly. Thus, in these cases, the resulting average *H/V* curve can be safely considered representative for the medium's volume underneath the array.

The modelling of both the dispersion and *H/V* ratio curves during the inversions was not restricted to the fundamental mode only, but the possibility that higher modes can participate to define the observed dispersion curve is allowed. During the inversion, the two data sets are weighted in a balanced way using the cost function proposed by Herrmann et al. (1999). Obviously, when one of the two experimental curves cannot be used (e.g. because of the presence of man-made industrial noise signals) the proposed inversion scheme can still be applied using only one of either the dispersion or *H/V* curves. In our cases, dispersion curve and H/V curves were both used at all sites with the exception of LGN and BZZ. At these two sites only dispersion curves were considered.

For further explanation on surface wave methodologies, see document: Project S4: ITALIAN STRONG MOTION DATA BASE, Deliverable # 6, Application of Surface wave methods for seismic site characterization, May 2009.

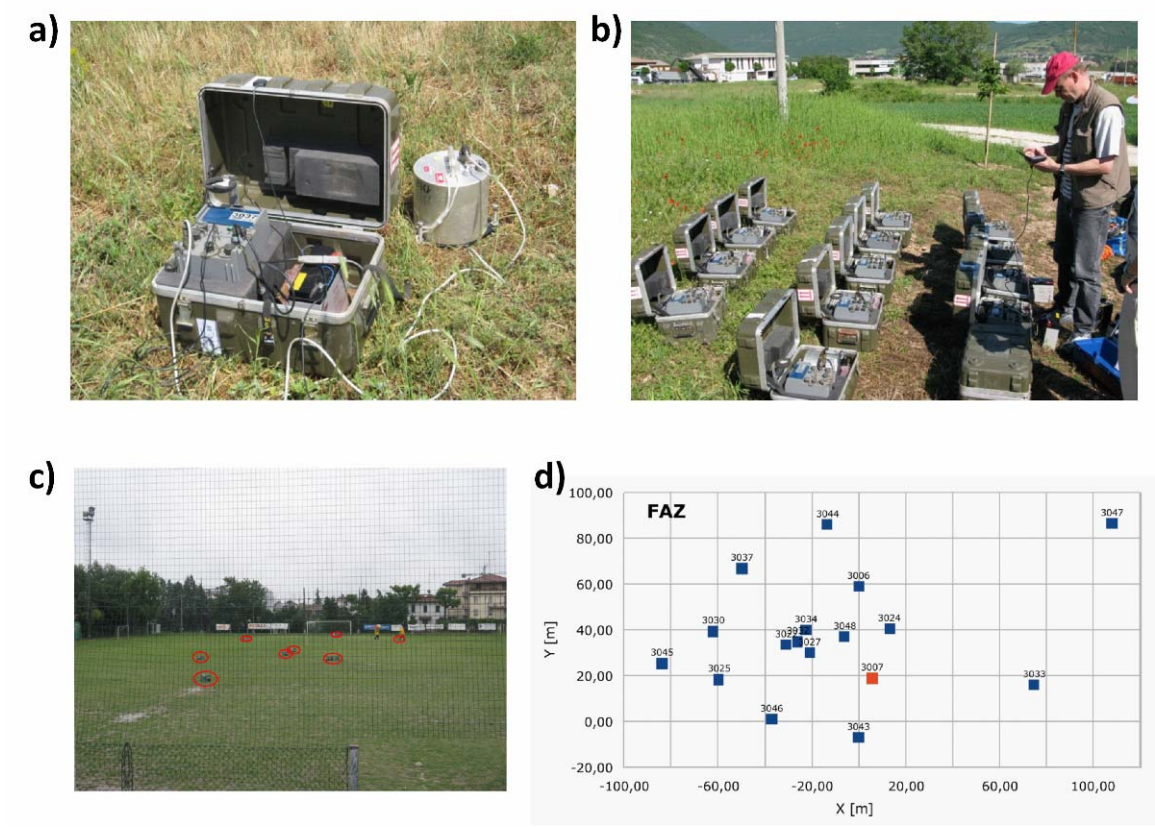

Figure 8 – a) Example of installation of an EDL acquisition systems plus Mark-L4-C-3D sensor. b) Set-up of the stations. c) and d) Example of array geometry in Faenza. d) shows also stations which worked properly (in blue) and those which had problems that therefore were excluded in the analysis (in red).

3.5. RU7 – University of Siena

Activities of RU7 focused on the seismic characterization of rock/stiff soil RAN sites. To this purpose, single station and array measurements of ambient vibrations were considered along with a detailed study of the local geological configuration deduced from specifying geological surveys. The major goal of performed activities was evaluating the feasibility of passive

seismic prospecting under strict geological control, to provide effective results. In fact the application of these procedures on rock/stiff soil sites poses specific problems that were to faced by developing peculiar procedures. These area discussed in detail in the Deliverable 11, devoted to this topic.

In general, the procedure was the following:

Detailed Geological survey of the study area resulting in a geo/lithologic map at the scale 1:5000 of the area surrounding the relevant RAN station. This also aimed at the evaluation of the degree of lateral heterogeneity present in the lithological structure paying major attention to faults and their relevant damage area

Extensive single station ambient vibration survey at the station and in the surrounding area to detect possible lateral variations potentially responsible for site effects

Ambient vibration measurements carried on with a seismic array at the RAN site or at a site representative of the subsoil configuration at the RAN site. In this last case, suitable inversion procedures and test were carried on to warrant the representativeness of ambient vibration measurements

Global interpretation of measurements to determine the Vs profile and of the resonance frequency at the RAN site by considering the whole set of collected data

Details concerning experimental tools and processing techniques are given in the following sections.

3.5.1. Single station measurements

The goal of this kind of measurements is the retrieval of the HVSR curve that represents for each frequency, the average ratio between Horizontal (H) to vertical (V) ground motion components of ambient vibrations (SESAME, 2004). Each single-station measurement was executed with a three-directional digital tromograph Tromino Micromed (see www.tromino.it) with a sampling frequency of 128 Hz and an acquisition time length of 20 minutes. This value represents a good compromise between the celerity of the measurement execution (which is one of the main merits of this technique) and its accuracy, according to the SESAME guidelines and other studies (see, e.g., Picozzi et al., 2005). To provide HVSR curves, the time series relative to each ground motion component was subdivided in non-overlapping time windows of 20 s. For each of these, the signal was corrected for the base line, padded with zeros, and tapered with a Bartlett window; the relevant spectrogram was smoothed through a triangular window with frequency dependent half-width (5% of central frequency) and the H/V ratio (HVSR) of the spectral components (the former being the geometric mean of North-South and East-West components) was computed for each frequency. Spectral ratios relative to all the time windows considered were then averaged, and a mean HVSR curve was computed along with the relevant 95% confidence interval.

Before interpreting HVSR curve in terms of subsoil dynamical properties, we checked the possible occurrence of spurious HVSR peaks (e.g., due to impulsive or strongly localized anthropic sources. To this purpose, we investigated both the time stability of spectral ratios over the recording length and their directionality. The latter was analyzed by estimating the HVSR curves derived by projecting the ground motion along different horizontal directions. If transient directional effects were identified in the directional HVSR curves, the relevant portions of the record were discarded.

This check was formalized into a classification procedure previously adopted in the ambient vibration surveys in the area damaged by the L'Aquila earthquake, whose criteria were shared by the research units anticipating in the project and is summarized in the Appendix.

3.5.2. Array Measurements

This technique consists in recording ambient vibration ground motion by means of an array of sensors (geophones) distributed at the surface of the subsoil to be explored (see, e.g., Okada, 2003). Relevant information concerning phase velocities of waves propagating across the array is obtained from average cross-spectral matrixes relative to sensor pairs. In the present analysis, plane waves propagating across the array were considered only. Since vertical sensors were used only, these waves are interpreted as plane Rayleigh waves in their fundamental and higher propagation modes. Determination of Rayleigh wave phase velocities V_R as a function of frequency (dispersion curve) from cross-spectral matrixes can be carried on in several ways. In the present analysis, the Extended Spatial Auto Correlation (ESAC) technique (Ohori et al., 2002; Okada, 2003) was applied. The basic element of this analysis is the cross-correlation spectrum deduced by the analysis of ambient vibrations measured at a couple of sensors $\phi\ (f,r)$ where f is frequency and r is the distance between the relevant sensors .

To this purpose, registrations relative to each sensor are partitioned in a number of non overlapping time windows of fixed duration (20 sec). Time windows characterised by energy bursts were removed from the analysis. To this purpose, a time segment is considered in the analysis if standard deviation of all the traces of that time window does not exceed the threshold fixed in advance for each trace. In general, this threshold was fixed to be 2 times the standard deviation computed over the whole registration for the relevant trace. In each accepted time window, the time series was detrended, padded and tapered (5% cosine windows). For each time window and couple of sensors, the cross spectrum was computed. The average cross spectrum was then computed for each couple of sensors by considering all the relevant time series. The resulting average cross-spectrum was thus smoothed in the frequency domain by a moving triangular window having a half-width proportional to the central value (usually 10%) and normalized to the relevant auto spectra.

In the assumption that ambient vibration wave field can be represented as a linear combination of statistically independent plane waves propagating with negligible attenuation in a horizontal plane in different directions with different powers, but with the same phase velocity for a given frequency, the normalized cross-spectrum $\phi_{ij}(f,r)$ relative to sensors located at a distance r, can be written in the form

$$\phi(f,r) = J_0\left(\frac{2\pi f r}{V_R(f)}\right)$$

where J_0 is the Bessel function of *0-th* order. In the ESAC approach, the value of V_R relative to each frequency f is retrieved by a grid search algorithm to optimize (in a RMS sense) the fit of the above function of r for the relevant frequency f (Ohori et al. , 2002; Okada, 2003). Uncertainty on "apparent" velocities was computed by means the second derivative of the misfit function relative to grid search procedure (see, Menke, 1989). However, since these estimates tend to be under-conservative in some cases, the lower bound of the confidence interval for experimental V_R values was fixed by using the relationship proposed by Zhang et al. (2004).

The $V_R(f)$ value obtained in this way, is the "apparent" or "effective" Rayleigh waves phase velocity that coincides with the actual phase velocity only in the case that higher modes play a negligible role. In the other cases, a relationship can be established between actual phase velocities and the apparent one (Tokimatsu, 1997).

The fact that the ESAC approach allows the determination of the apparent dispersion curve instead of the modal ones could represent an important limitation of this procedure with respect to other approaches (e.g., f-k techniques). On the other hand, this makes the approach

here considered more robust with respect to the alternative procedures, since it does not require troublesome picking of existing propagation modes.

In the present study, ambient vibrations were recorded for 20 minutes at a 256 Hz sampling rate by using 16 vertical geophones (4.5 Hz) and a digital acquisition system produced by Micromed (http://micromed.com/brainspy1.htm). Geophones were placed along two crossing perpendicular branches (with maximum dimensions lower than 100 m) and irregularly spaced (in the range 0.5-30 m).

3.5.3. Inversion

HVSR and apparent V_R curves have been jointly inverted to constrain to the local Vs profile. To this purpose, a genetic algorithm procedure was considered. This is an iterative procedure, consisting in sequence of steps miming the evolutionary selection of living being (see Picozzi and Albarello, 2007 and references therein). The formalization proposed by Lunedei and Albarello (2009) was used as the forward modelling implemented in the procedure. This procedure assumes the subsoil as a flat stratified viscoelastic medium where surface waves (Rayleigh and Love with relevant higher modes) propagate only. From this model, both theoretical HVSR and effective dispersion curves can be computed from a set of parameters representative of the hypothetical subsoil (V_S, V_P, density, Q_P and Q_S profiles). The discrepancy between theoretical and observed HVSR and dispersion curves were then evaluated in terms of a suitable misfit function, strictly linked to the well-known χ^2 function, and that allowed different choices about the combination of the discrepancies of V_R and HVSR curves, with different weights as well. The confidence interval around preferred Vs values and layer thickness were evaluated by following Picozzi and Albarello (2007).

4. Case histories

In this section some selected case studies are reported, in order to show the application of methodologies previously described.

4.1. UR2 – INGV Roma

As an example of the UR activities, we present the work on the R.A.N. site of Rieti (RTI, lat. 43.831 – lon. 12.829). The site is located in the Rieti alluvial basin, a typical intermountain Apennines' basin crossed by the Velino River that flows in the South – North direction. The area presents a very flat morphology due to the presence of lacustrine Holocene deposits related to an old lake drained starting from 271 a.C., through the opening of an artificial channel in the NW side of the area in correspondence of the of Marmore falls. The basin is surrounded by mountain ranges consisting of outcropping rocks, mainly of Eocene time. Limestone is also outcropping in small hills aligned in the western sector of the basin (Colle San Balduino, Montisola). In the SouthWestern part of the basin an extended plate of Pleistocene Travertine deposits. This unit can reach a thickness of few tenths of meters and represents the outcropping formation in the SouthEastern part of the basin, including the historical centre of Rieti, the main town in the area. Figure 9 shows a shaded relief map of the area and a picture of the field used for the arrays deployment.

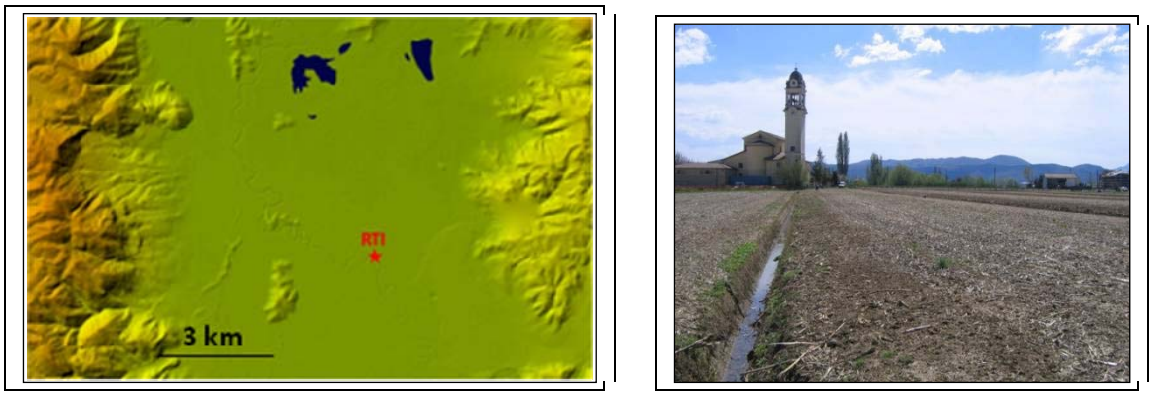

a) b)

Figure 9 – a) shaded relief map of the Rieti basin (left), the red star shows the position of R.A.N. – RTI strong motion station located in the Chiesa Nuova neighborhood. b) picture of the site selected for MASW measurements.

Due to lack of space, the area where the R.A.N. station is installed does not allow to perform any array measurement. Consequently we had to move into an open field close by (150-200 meters) to install both 1D and 2D arrays.

The 1D array was composed by 72 sensors with a spacing of 2 meters for a total length of 142 meters. The array was energized by minigun shots with offset of 40, 20 and 0 meters at both sides of the deployment. An extra shot point was chosen at the centre of the array. For every offset two shots were performed. Data sampling rate was set at 0.125 ms, recording window duration was of 2 seconds.

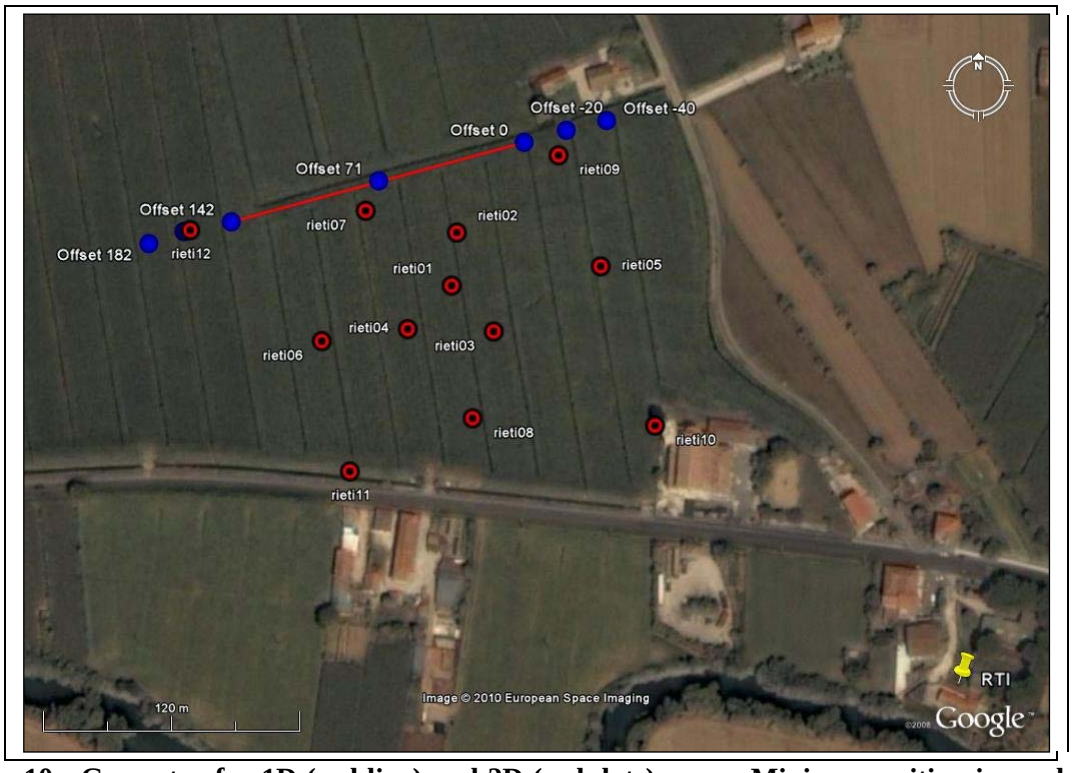

Figure 10 - Geometry for 1D (red line) and 2D (red dots) array. Minigun position is marked by blue dots. The green marker indicates the R.A.N. (RTI) station.

Using the same array configuration 10 seismic noise windows 30 seconds long were recorded for the passive technique. Some extra window was also recorded while a van was moving at the eastern end of the deployment. In this case data sample was set to 2 ms.

The 2D array was based on 12 stand alone stations recording continuously during a 2 hours time window with a sampling rate of 5 ms. Absolute timing was obtained by GPS clock, while the exact position of measuring points was derived by a GPS differential kinematic survey. The array layout was the one described in the previous section; the array maximum aperture was of about 235 meters. Figure 10 shows the geometry of the arrays and the location of shots.

The 2D array stations were first used for evaluating microtremor spectral ratios by means

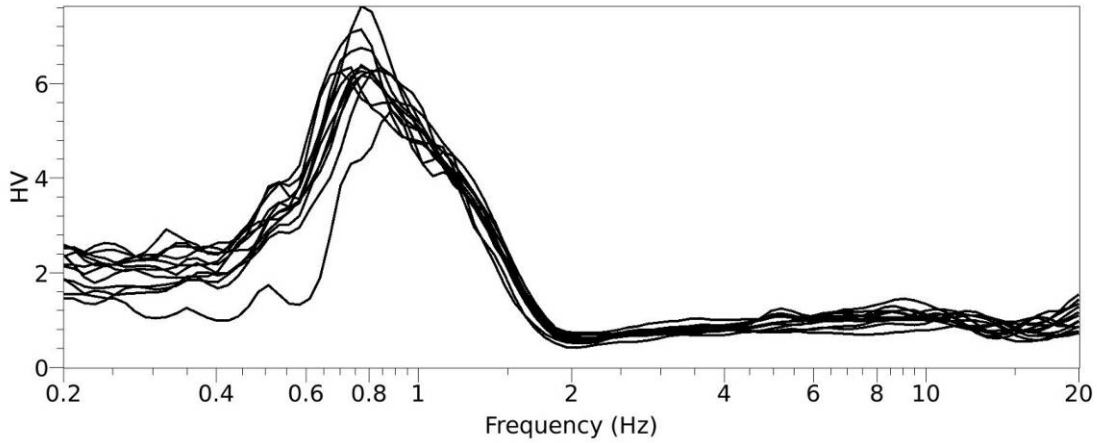

Figure 11 - HVNSR spectral ratio for the stations of the 2D array.

of HVNSR technique. The results of this analysis are shown in Figure 11 that indicates a clear amplification peak in the frequency range of 0.7 - 0.8 Hz. The stability of this peak supports the hypothesis of a 1D behavior of the site. As an example of the quality of data, Figure 12 shows a data section for the active experiment.

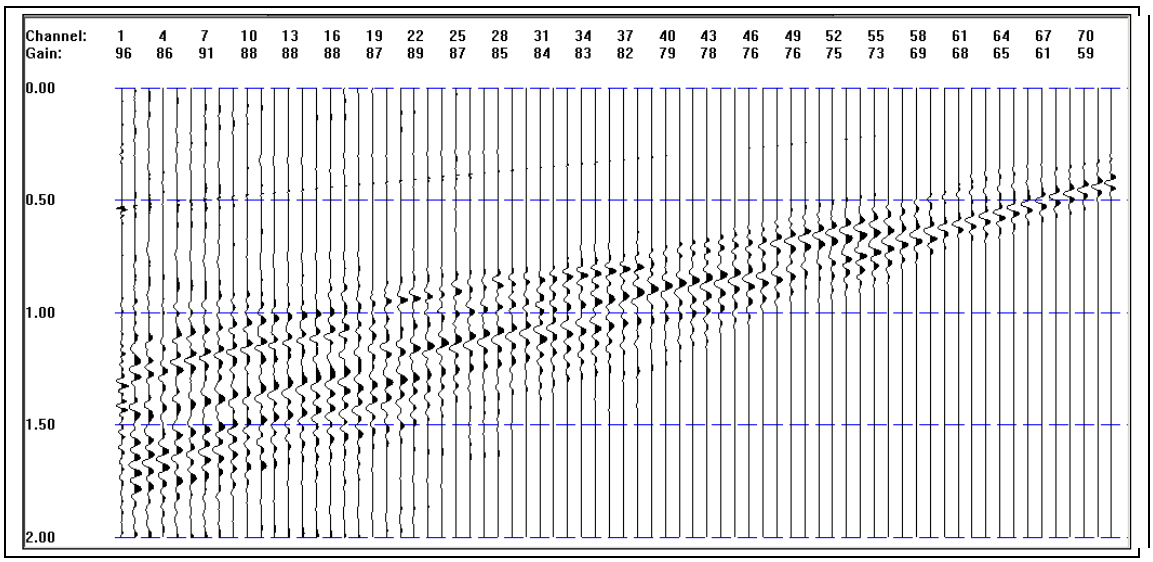

Figure 12 - Seismic section for a reverse shot with an offset of 40 meters.

To define the dispersion curve we first analyzed active data. All the software described in the previous section was utilized with very consistent results. As an example we present the analysis performed with the Optim software to derive the experimental dispersion curve in the frequency - slowness domain for a 40 meters offset shot (Figure 13). It is clear the presence

of two branches in the curve probably related to the fundamental Rayleigh waves mode and to a higher mode. The dimension of the region of maxima can give an idea about the uncertainties in picking.

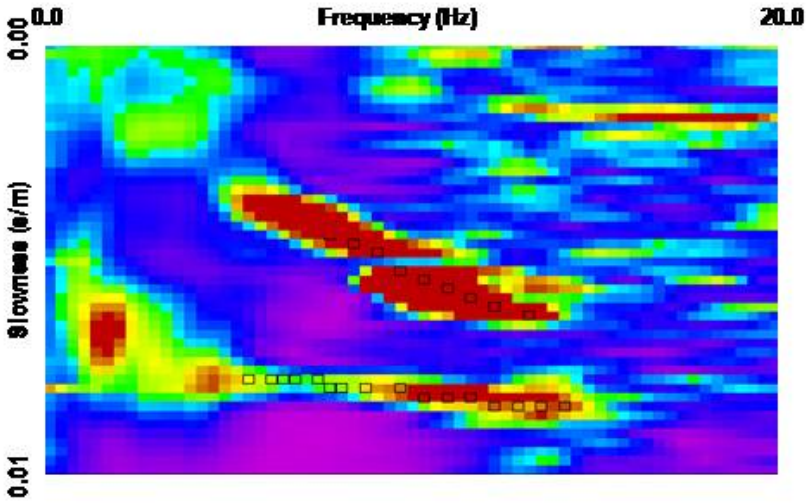

Figure 13 - Frequency – slowness plane and dispersion curve (black squares) picking for active source (offset 40 meters).

In order to better explore the low frequencies range we analysed passive 1D data as shown in Figure 14. In this case the picking is done on the lower envelope of maxima regions to take into account the presence of wave fronts crossing the array with some angle, i.e. with apparent velocity higher than the real one according to Louie (2001).

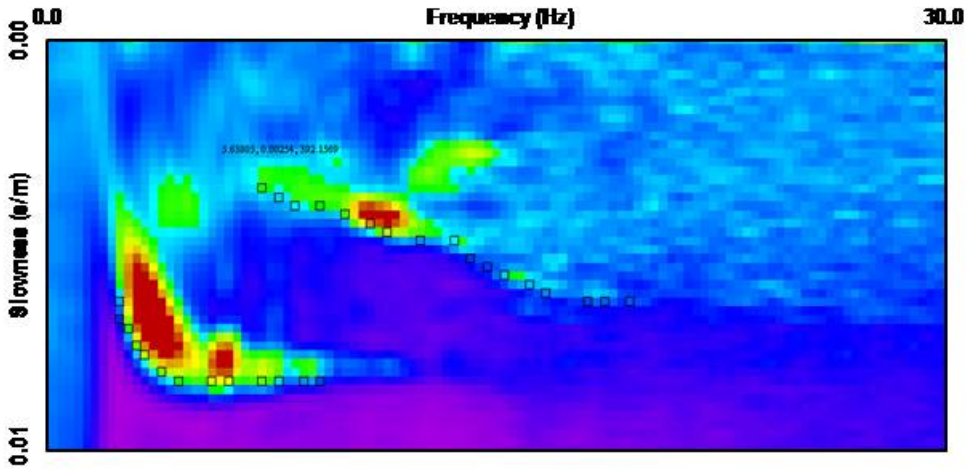

Figure 14 - Frequency – slowness plane and dispersion curve (black squares) picking for passive source (offset 40 meters).

The results obtained with the use of the moving van are showed in Figure 15. Also in this case the picking is performed in the maxima region since the source was aligned to the array. All the analysed data produce very similar results. Moreover, the passive technique is able to better explore the low frequency range.

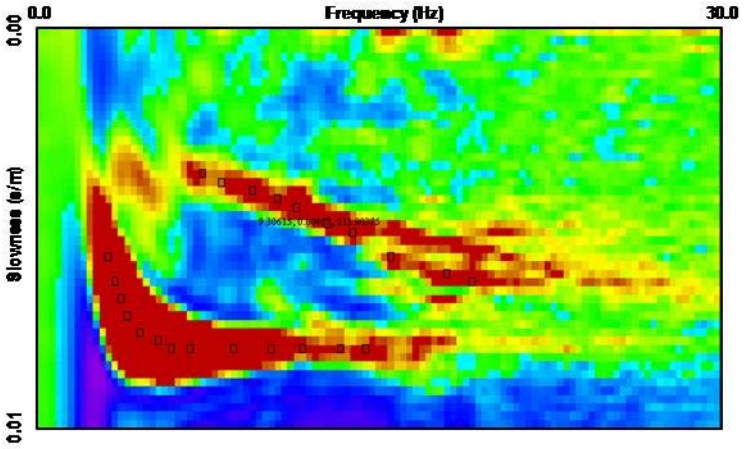

Figure 15 - Frequency – slowness plane and dispersion curve (black squares) picking for moving vehicle source (offset 50 meters).

To improve the low frequency detection we applied conventional fk, high resolution fk and MSPAC techniques to the 2D passive array data. In this approach, considering the geometry of the array, the resolution can be considered good in the 1.5 - 3.5 Hz frequency range as shown by the curves (solid black and dashed) shown in

Figure 16 along with the dispersion in the frequency – slowness plane. The results obtained by the use of MSPAC technique are also very similar and consistent.

To summarize we present in

Figure 17 we present the dispersion curve obtained by merging all the results obtained using 1D and 2D active and passive data.

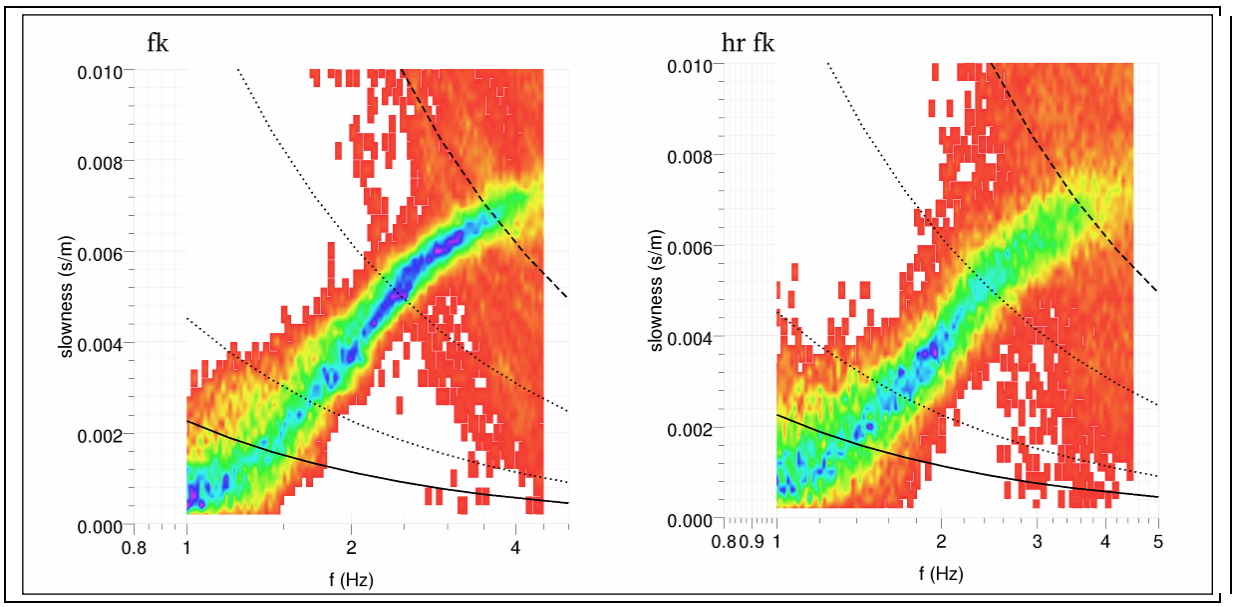

Figure 16 - Conventional and high resolution 2D analysis on passive data.

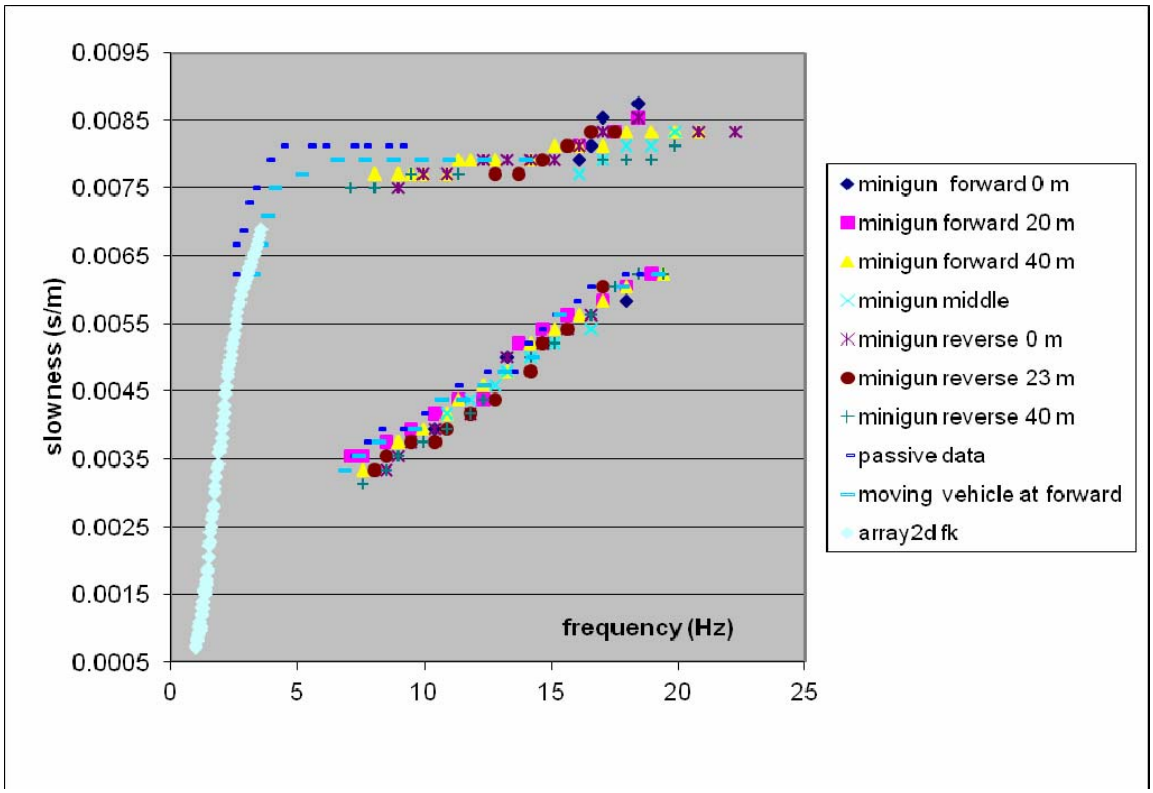

Figure 17 - Experimental dispersion curve for all the performed measurments.

The dispersion curves of

Figure 17 were inverted using the Geopsy code as described in the previous section. The possibility of fitting both fundamental and higher Rayleigh wave modes was used. A further constraint to the inversion was introduced using of the ellipticity function. In fact we tried to reproduce also the ellipticity of Rayleigh waves as derived by H/V spectral ratios. The results of the joint inversion are shown in

Figure 18 and Figure 19 that shows both Vp and Vs profiles. It is clear a low velocity layer (Vs < 200 m/s) with a thickness of about 60 meters over imposed to a layer with velocity of about 500 m/s. The seismic bedrock probably is not well constrained but it is found at a depth higher than 150 meters.

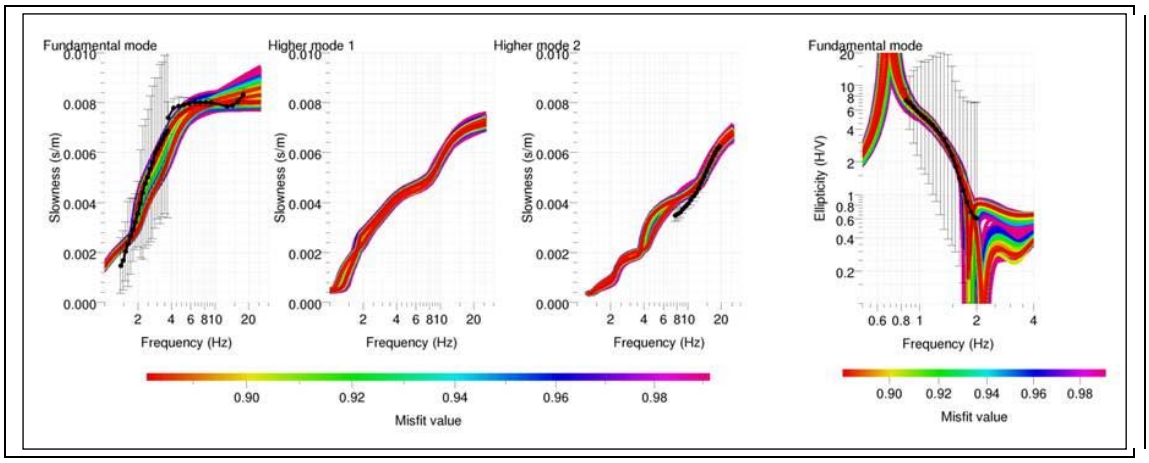

Figure 18 - Comparison between experimental and modeled dispersion curves and Rayleigh waves ellipticity function.

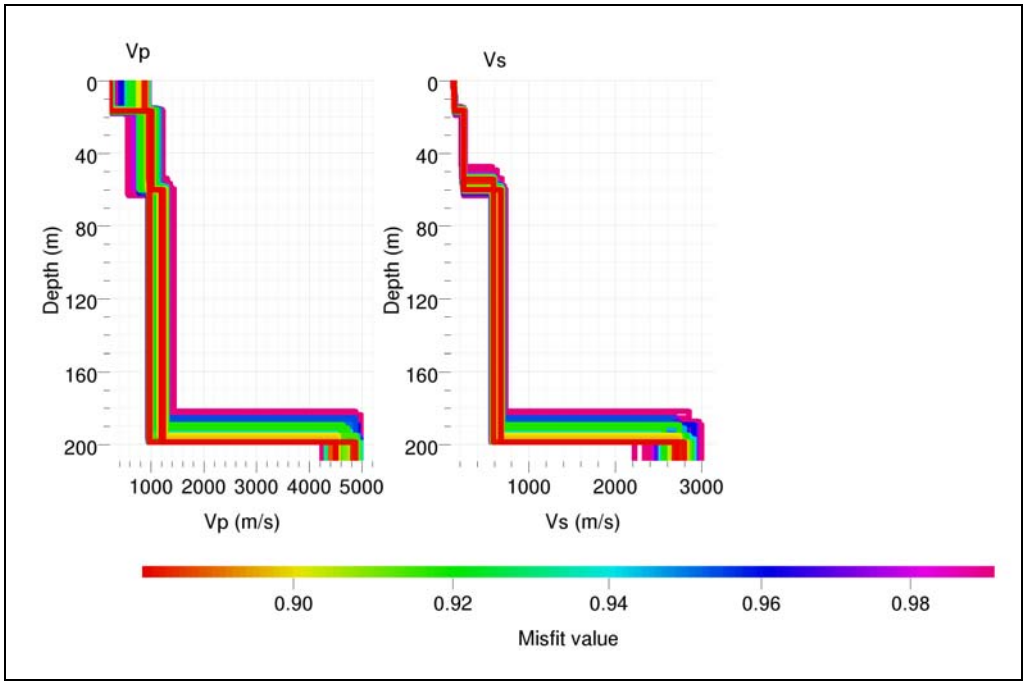

Figure 19 - Vp and Vs best fit models from the dispersion curve inversion.

The agreement between experimental and modelled (figure 4.12) data is quite good probably due to the site conditions. In this case the 1D hypothesis is completely fulfilled and the soil characteristics consent a good coupling of the active source with the ground and a good transmission of seismic signals. As final remark for the investigated site the MASW technique turned out to be a useful tool for site characterization.

4.2. UR4 – Politecnico di Torino

In the following paragraph two case histories among the sites investigated by Politecnico di Torino are presented: Catania Piana (station code CAT) and Noto (station code NTE). Catania Piana acquisition campaign involved both active and passive Surface Wave measurements, while in Noto site active tests were sufficient to retrieve the seismic bedrock depth, being the interface between the seismic bedrock itself and the weathering layers quite shallow. Other case histories are reported in Bergamo et al. (submitted).

4.2.1. Site description – CAT (Catania, CT, Italy)

Catania Piana RAN station lies on the alluvial plain of Catania, approximately 3.5 km from the sea. Catania Plain is made up of alluvial deposits with a substantial percentage of clay decreasing with depth where it is progressively substituted by sand: moreover, many gravel or sand lenses are present. No shallow seismic bedrock is expected for CAT site, but a sequence of soft layers made up of alluvial deposits with a S-wave velocity increasing with depth.
The map and site location are shown in Figure 20 and Figure 21. The Geological map of the Catania Piana area is presented in Figure 22.
Goal of the seismic tests is the estimation of the S-wave velocity profile of the subsoil. Both passive and active surface wave tests were performed in order to increase the investigation depth, as no shallow seismic bedrock is expected.

Figure 20 – Catania (Piana): site map.

Figure 21 – Catania (Piana): site location and active measurement array

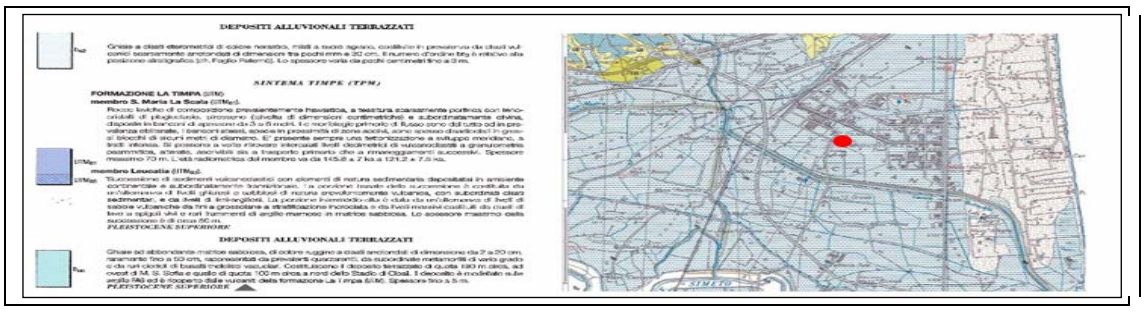

Figure 22 - Geological map of Catania area. The position of the RAN station is indicated by red dot.

Acquisition geometry is shown in Figure 5, receivers characteristics are described in Table 1. 48 receivers were used for active tests, with a spacing of 1.5 m between neighboring geophones, so that the total length of the array is 70.5 m. A relatively large spacing between geophones (1.5 m) was chosen both because of the wide extent of the area where the survey was performed and because of the required investigation depth: as no shallow seismic bedrock is expected, a larger spacing ensures a greater investigation depth. 16 receivers were used for passive tests: one three components geophone was placed at the centre of the array

and three others were disposed along a circle whose radius is 9 m; 12 vertical geophones were arranged along the outer circle whose radius is 25 m.

Active and passive data were processed according to procedures described in paragraphs 3.3.2 and 3.3.3. Figure 23 shows the f-k spectrum obtained from active tests.

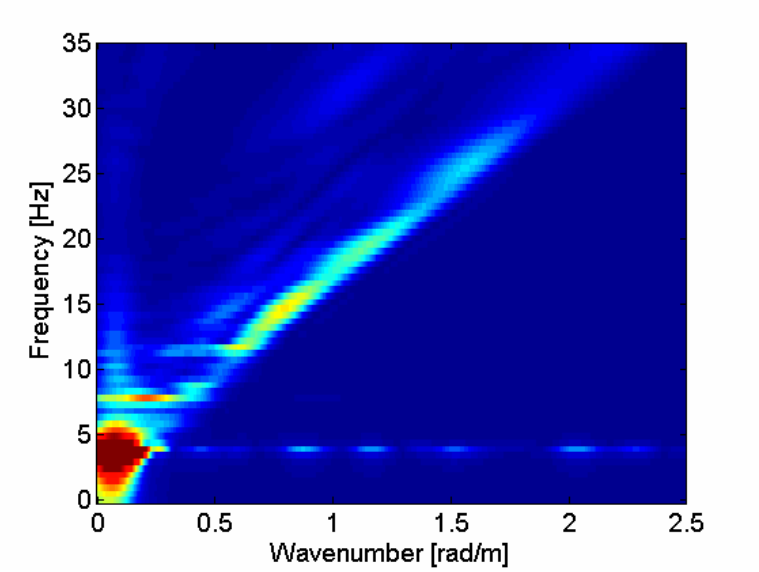

Figure 23 - Catania (Piana) . F-k spectrum from active data.

Figure 24 portrays the obtained experimental dispersion curve, with a distinction between points from active and passive measurements. Note the good matching between blue branches (points from passive measurements) and black branches (points from active measurements).

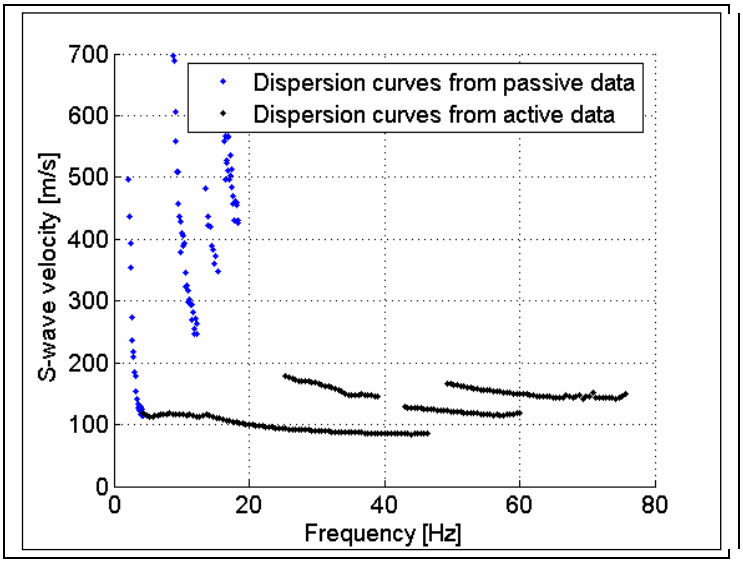

Figure 24 – Catania (Piana) . Experimental dispersion curve.

The apparent dispersion curve is characterized by the presence of four propagation modes: all of them show a steep velocity increase in the low frequency range. It should also be noticed that the low frequency part of the dispersion curve has been retrieved by processing passive data which allow a greater investigation depth.

Data were inverted using a multimodal stochastic approach (see paragraph 3.3.4), the best fitting profiles are plotted in Figure 26 a), profile colour depends on the misfit, from yellow to

blue (best fitting profile). In Figure 26 b) the best fitting profile is compared with the results of a SDMT test and of a Down-hole test previously performed in the environs of Catania Piana site. It is important to point out that the DHT was performed at the same location of surface wave testing, hence the comparison is more appropriated. The SDMT (Seismic Dilatometer Test) on the contrary was performed about 3 km away, hence the comparison is not strictly applicable. Nevertheless the result is reported in the graph because the shallow clayey formation is very homogeneous throughout Catania plane, hence, at least for the shallow portion. Surface wave method results are in fairly good agreement with the SDMT and DH tests profiles. In particularly for the shallower part of the profile the agreement with SDMT is very good, whereas the trend of increasing velocity with depth is compatible with the one detected by DHT. In Figure 25 the experimental dispersion curve is compared with the determinant surface of the best fitting model.

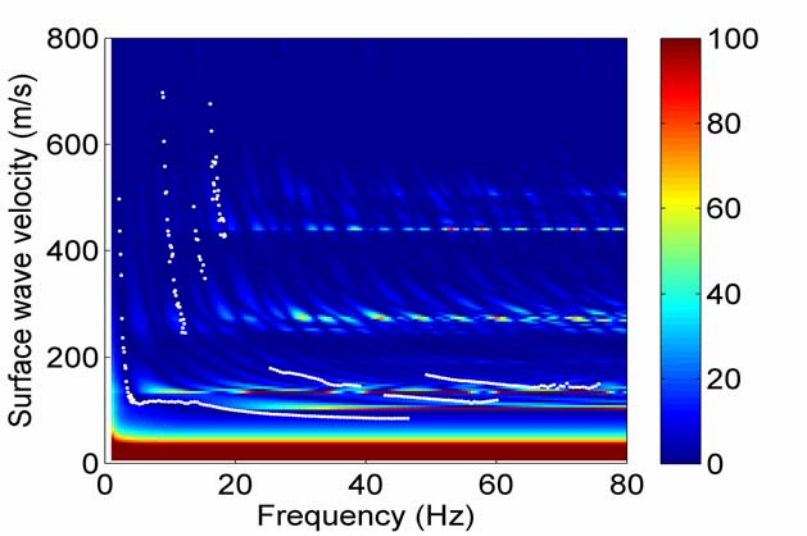

Figure 25 - dispersion curve compared with the misfit surface of the best fitting model

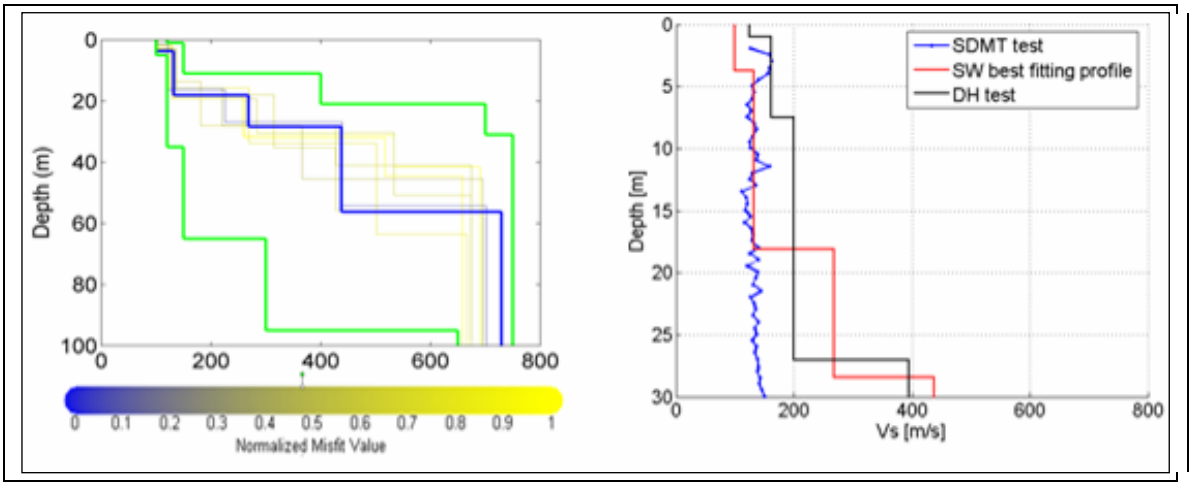

Figure 26 Catania (Piana) – a) Monte Carlo results (from yellow to blue) of the inversion with the boundaries (green). b) Catania (Piana) – Best fitting profiles compared with the SDMT and DH tests results provided by Università di Catania.

Vs (m/s)	Thickness (m)	Poisson coefficient	Density (T/m^3)
100	3.7	0.3	1.8
132	14.4	0.3	1.8
268	10.3	0.3	1.8
438	27.8	0.3	1.8
730	-	0.3	1.8

Table 3 - Catania Piana: subsoil parameters of the best fitting profile.

The best fitting profile shown in Table 3 suggests a Vs30 of 160 m/s for Catania Piana, no seismic bedrock was detected. The site can thus be classified as D site according to EC8 classification.

4.2.2. Site description – NTE (Noto, SR, Italy)

Noto (NTE) RAN station is classified as rock outcrop and a very limited zone of rock alteration and vegetation soil was expected above the calc-tufa seismic bedrock (see Figure 27). NTE site is located on the Hyblean Plateau, within an area whose subsoil is marked by the presence of the Hyblean Foreland carbonate sequence. The map of the measuring array and of the site location is shown in Figure 28.

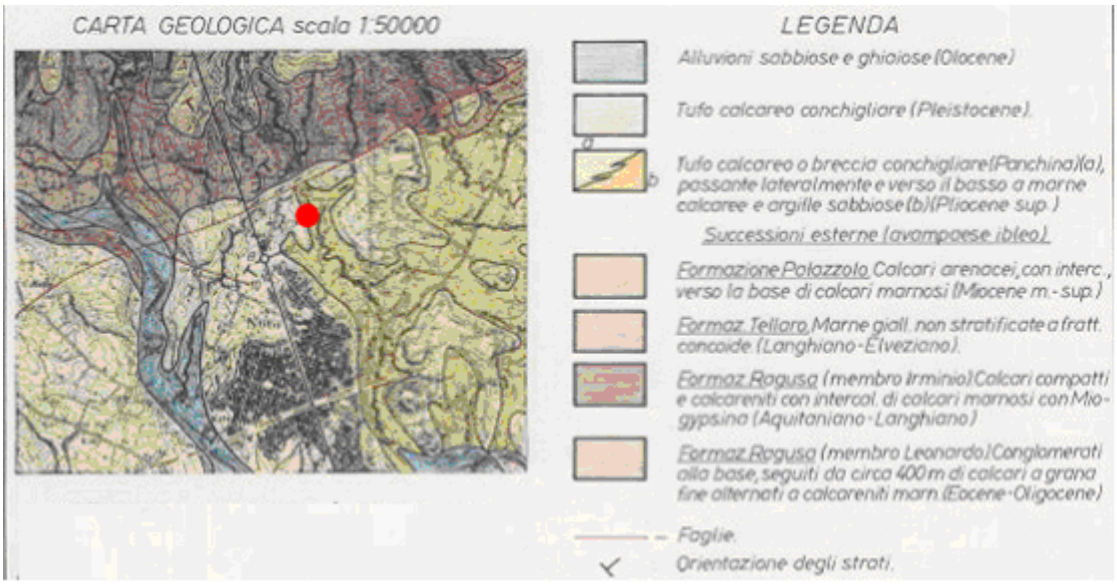

Figure 27 - Geological map of Noto area. The position of the RAN station is indicated by red dot.

An active survey only was performed because of the limited extent of the area surrounding the Noto RAN station. Also, since shallow seismic bedrock is expected, passive measurements are probably not necessary. The acquisition geometry was influenced by the limited extent of unpaved area on the site: a 24-receiver array was arranged with spacing between geophones of 0.8 m. The effectiveness of the survey however was not negatively affected by the short extent of the array: shallow seismic bedrock was expected, so that even a 18.4 m long survey line could ensure a sufficient investigation depth.

Figure 28 – Map of the array and station location

Acquired active data were processed by means of an f-k analysis (see paragraph 3.3.2). Figure 29 portrays the obtained f-k spectrum.

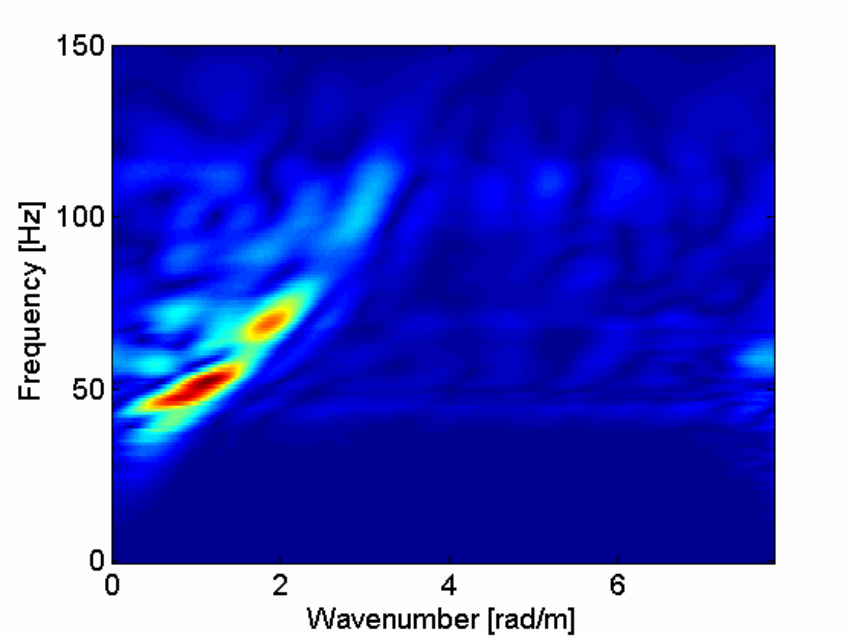

Figure 29 – Experimental f-k spectrum.

The retrieved experimental dispersion curve is shown in Figure 30; it is composed of a main branch and two small branches with higher velocities: note that the main branch shows a steep velocity increase in the low frequency range probably due to a jump on the first higher mode in that range. This jump is probably due to the strong velocity contrast between the seismic bedrock and the shallower layers. All branches were used for the inversion.

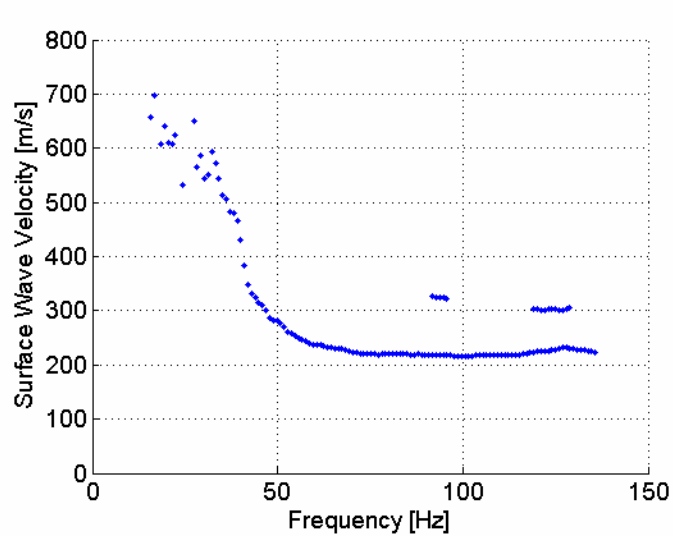

Figure 30 – Experimental dispersion curve.

The experimental dispersion curve was inverted with a Monte Carlo approach (see section 3.3.4). The best profiles are represented in Figure 31; all profiles are characterized by a 2 m weathering layer with a shear wave velocity of about 230 m/s: then velocity increases progressively with depth until a 900 m/s seismic bedrock is met at about 8 m depth. The best fitting profile is described in Figure 31.

Vs (m/s)	Thickness (m)	Poisson coefficient	Density (T/m^3)
231	1.8	0.3	1.8
343	1.6	0.3	1.8
520	2.6	0.3	1.8
668	1.6	0.3	1.8
870	-	0.3	2.0

Table 4 Noto: subsoil parameters of the best fitting profile

Figure 32 portrays the fairly good fitting between the experimental curve and the misfit surface of the best fitting mode: note that the experimental points fall in the minima of the determinant surface, and the low frequency part of the experimental dispersion curve tends to jump on the first higher mode, probably due to the impedance contrast between topsoil and calc-tufa seismic bedrock.

According to the profile shown in Figure 31, Noto NTE site is characterized by a Vs30 of 658 m/s: f0 is then computed as $V_{S,h}/(4h)$ = 13 Hz, where $V_{S,h}$ is the inverse of the average slowness from the surface to the seismic bedrock and h is the seismic bedrock depth. Noto NTE site can then be classified as B site according to EC8 classification.

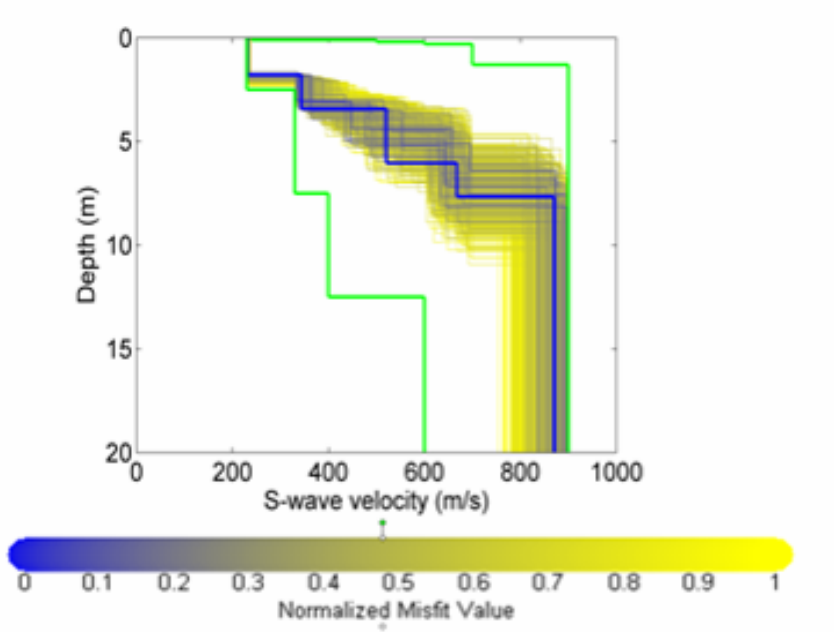

Figure 31 – Best fitting S-wave profiles.

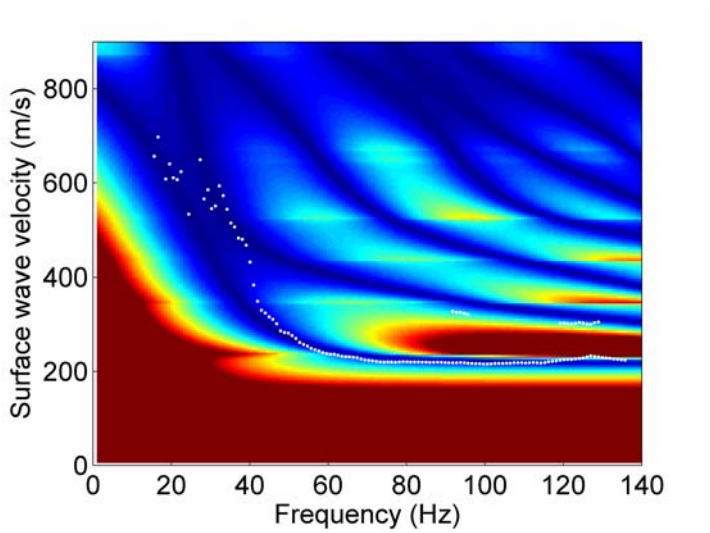

Figure 32 – Experimental dispersion curve compared with the misfit surface of the best fitting mode

4.3. UR8 – Helmholtz Centre Potsdam GFZ

4.3.1. Site description – CTL (Cattolica, RN, Italy)

The CTL station of the RAN seismic network is placed at the south-western outskirts of the city of Cattolica (Italy), within the alluvial basin – that here reach a depth of several hundred meters – made by the Po river. The array measurements could not be carried out nearby the accelerometric station. However, considering the geological characteristics of the area, the shear wave velocities structure is not expected to change significantly in over short distances. For this reason, in due to the logistic, the array measurements were carried out in a soccer field at a distance of about 250m from the seismic station (Figure 33).

a) 

b) 

Figure 33 - a) Position of the array measurements with respect to the CTL station. b) The field measurements.

4.3.2. Example of the complete workflow

The seismic array was composed by 17 stations (Figure 34). However, due to malfunctioning, only the data of 14 stations (grey circles in the Figure 34) could be used for the processing. The intra-station distances in the array ranged between 5.4 m to 115 meters.

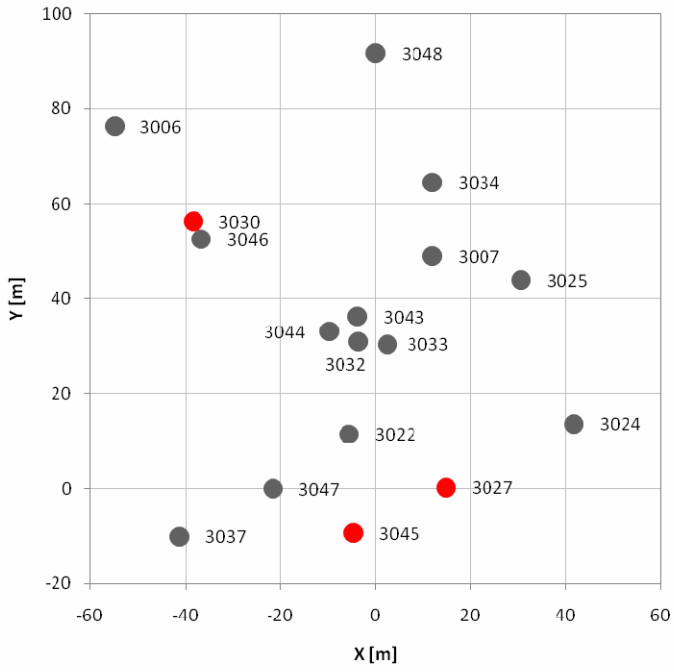

Figure 34 - Geometry of the array. Stations which had problems are evidenced in red.

The first step of the analysis consists in a visual inspection of the recordings at all stations. In particular, in order to identify malfunctioning of one station or channel and to select signal windows suitable for the H/V analysis, the quality of the recording was evaluated (1) analysing the signal stationarity in the time domain (Figure 35a), (2) the relevant unfiltered Fourier spectra (Figure 35b), and (3) the *H/V* variation over time (Figure 35a).

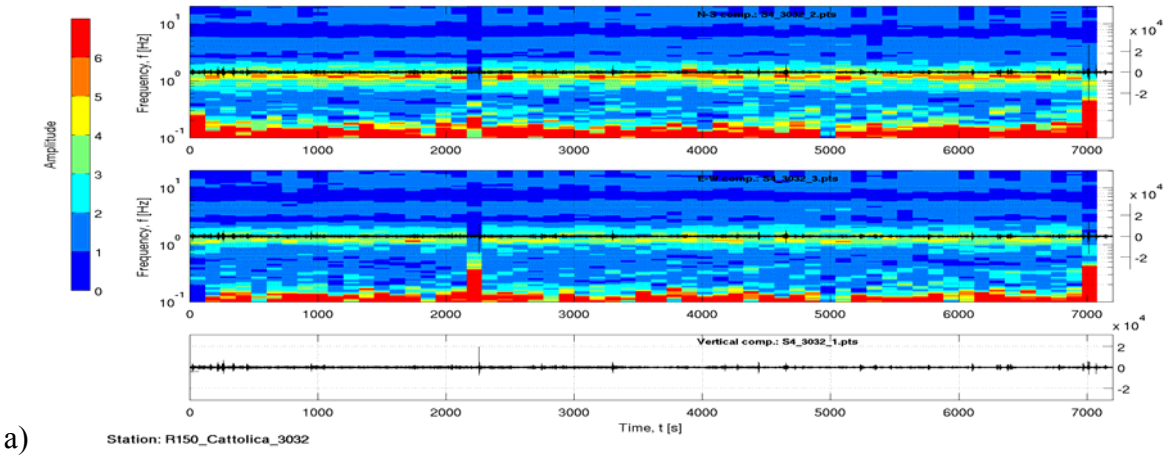

a)

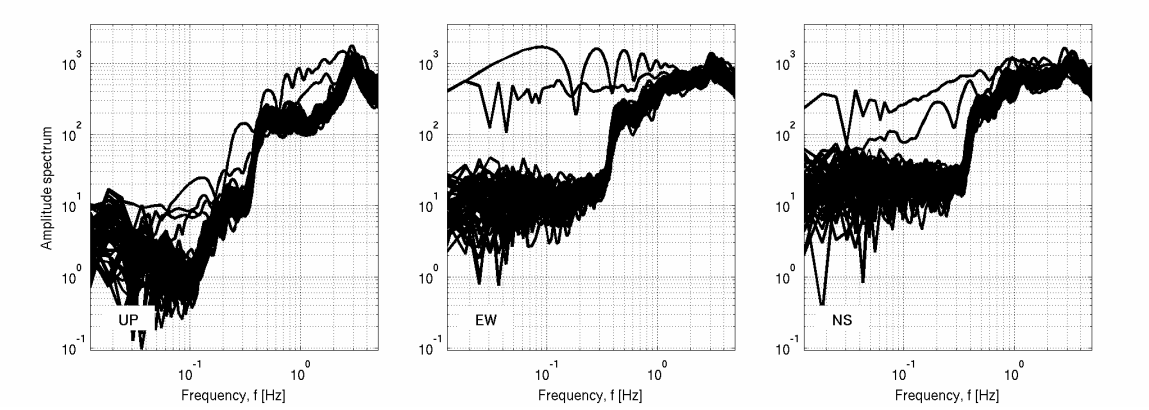

b)

Figure 35 – a) *H/V* spectral ratio versus time and corresponding time histories for station 3032. b) Fourier spectra for each of selected window. at station 3032. Left) Vertical component spectra, centre) E-W component spectra, right) N-S component spectra.

For each of the used 14 stations, 44 synchronized signal windows of 60 seconds were selected, avoiding windows affected by local disturbance. These windows were in turn used to estimate the experimental Rayleigh-wave dispersion curves (using the vertical component of ground motion only) both by f-k and ESAC analysis.
The ESAC Rayleigh-wave dispersion curve was obtained minimizing the root mean square (RMS) of the differences between the experimental and the theoretical Bessel function values (Figure 36). Values that differs more than two standard deviations from those estimated for the best fitting functions (red circles in Figure 36) are automatically discarded and the procedure iteratively repeated. Furthermore, data are discarded also when their relevant wavelength is shorter than the inter-station distance.

The f-k analysis offers the opportunity to verify if the requirements on the noise source distribution necessary for the application of the ESAC method were fulfilled. Figure 37 shows examples of the results of the frequency-wavenumber analysis (Maximum Likelihood Method) for several frequencies. The S-wave velocity of each frequency is estimated by the maximum shown in the plot like those in Figure 37.

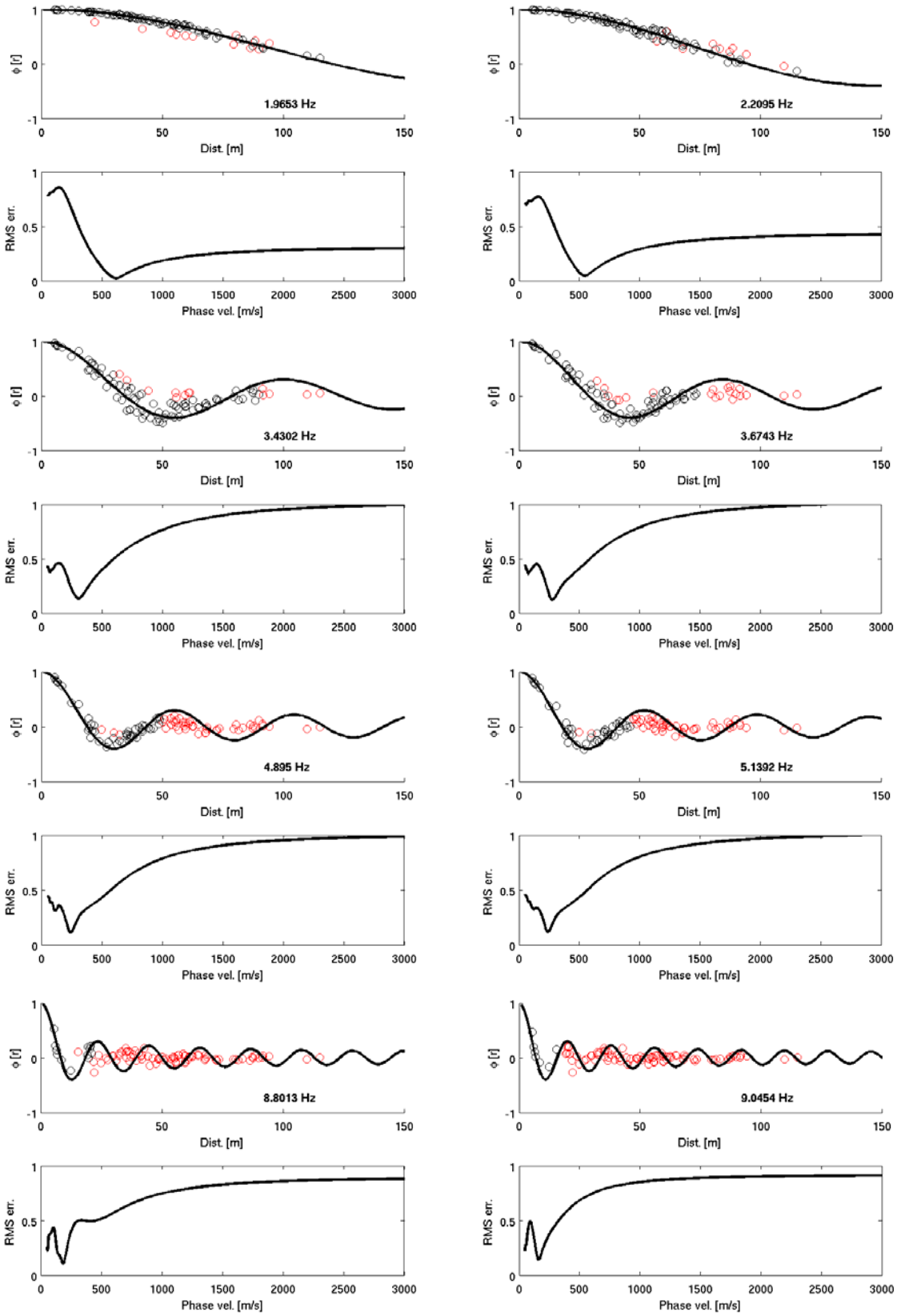

Figure 36 - Experimental space-correlation function values (circles) for different frequencies. The red circles indicate values discarded. The black lines depict the estimated space-correlation function values for the phase velocity showing the best fit to the data. The bottom panels show the relevant root-mean square errors (RMS) versus phase velocity tested.

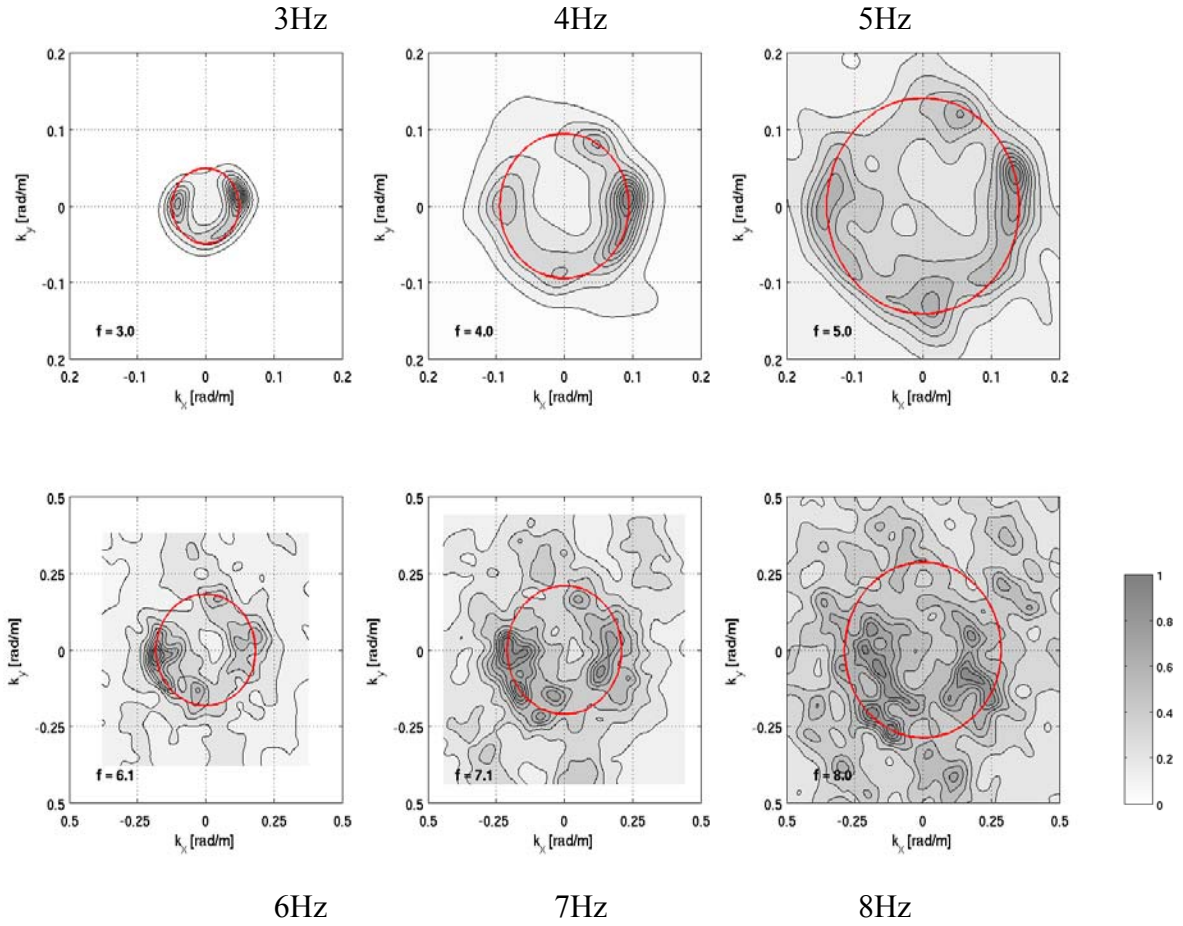

Figure 37 - f-k power density function at different frequencies. The red circles joints points with the same *k* value, corresponding to the maximum used to estimate the phase velocity.

Figure 38 shows the good agreement between the Rayleigh wave dispersion curves estimated both with ESAC and f-k approaches. Only below 3 Hz the f-k analysis provide larger phase velocities. The disagreement toward the lower frequencies confirms the results of previous studies (Parolai et al., 2007).

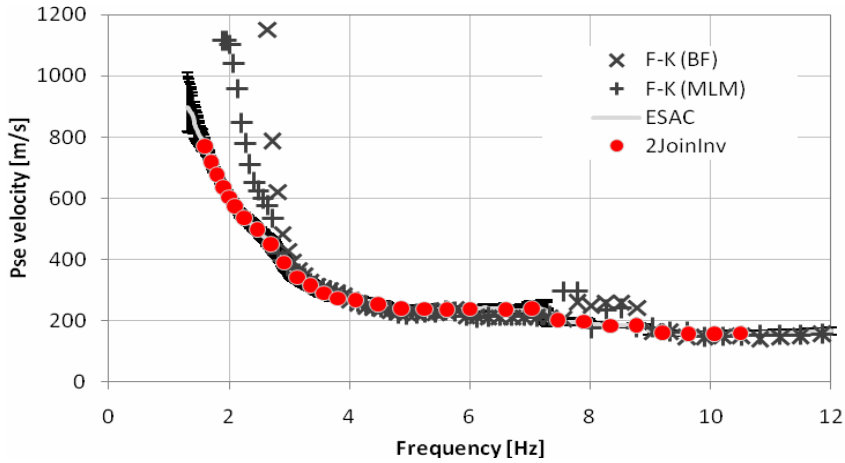

Figure 38 - Comparison of experimental phase velocity estimated by the ESAC method and by the f-k method (both for Beam Forming and Maximum Likelihood Method). The red circles represent the values used for the joint inversion. The intervals (Black lines) around the observed ESAC phase velocities are obtained by calculating the square root of the covariance of the error function.

An average *H/V* for each station was compute by averaging the H/V calculated for each signal window (Figure 39a). After having checked their similarity, the average H/V curves for each station were in turn averaged to obtain a single H/V spectral ratio representative for the array (Figure 39b). This average H/V was then used as input in the joint inversion procedure for the estimation of the S-wave velocity profile (red circles in Figure 39b).

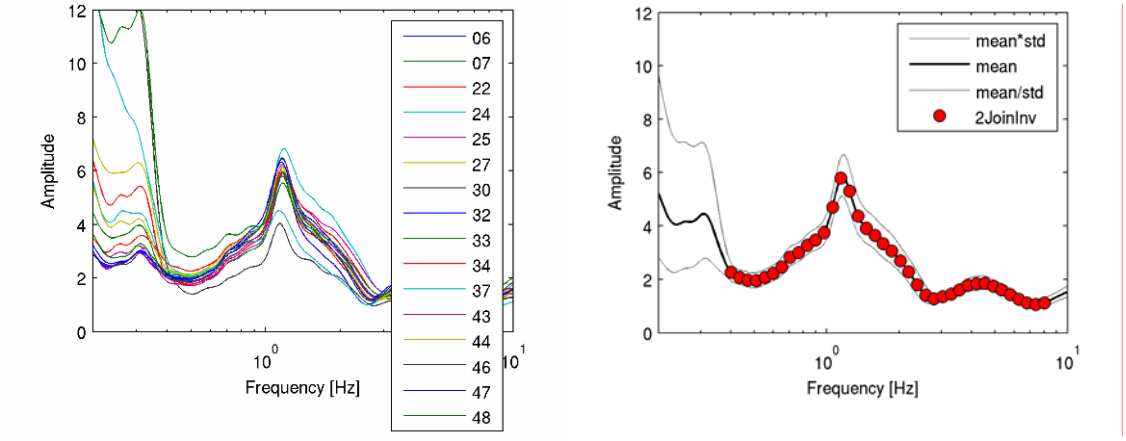

a) b)

Figure 39 - a) average *H/V* for each station of the array (e.g. 06 stands for station 3006, 32 stands for station 3032, etc.) and b) the average H/V of the array. The red circles represent the values used in the inversion procedure.

The inversion of dispersion and *H/V* curves to estimate the S-wave velocity profile was carried out fixing to 7 the number of layers overlying the half-space in the model (Table 5). Through a genetic algorithm a search over 80000 models was carried out and the agreement between the theoretical *H/V* and Rayleigh-wave dispersion curves with the observed ones was evaluated by means of a cost function (see above). The inversion was repeated several times starting from different seed numbers, i.e. from a different population of initial models. In this way it was possible to better explore the space of the solution. In the inversion process, the possibility that higher modes might participate to define both the dispersion and the H/V curve was allowed.

	Shear wave velocity, V_S [m/s]		Thickness, h [m]		Density, ρ [ton/m^3]
Layer	MIN	MAX	MIN	MAX	
#1	100	250	5	20	1.9
#2	150	400	10	40	2.0
#3	250	650	20	80	2.1
#4	300	800	30	120	2.1
#5	400	900	50	200	2.2
#6	400	900	50	200	2.2
#7	500	1200	250	1000	2.2
Half-space	1000	2500	Infinite		2.3

Table 5 Parameters ranges used to joint inversion.

During the inversion procedure the thickness and the shear wave velocity for each layer could be varied within the pre-defined ranges. On the contrary, for each layer, density was assigned *a priori*, while P-wave velocity (V_P) was calculated through the values of the S-wave velocity Vs via the equation: $V_P\,[m/s] = 1.1 \cdot V_S + 1290$, proposed and validated for deep soil deposits

by Kitsunezaki et al. (1990). In the cost function used, after trial and error test, the weight of 0.05, that allowed the best balanced fit of dispersion and H/V curves, was adopted.

4.3.3. Discussion of the results

In Figure 40a all the tested models during the inversion are depicted (gray lines). The best fit model (white line) and the models lying inside the 10% range of the minimum cost (black lines) function are highlighted. The agreement between experimental and theoretical Rayleigh wave dispersion curves (Figure 40c-d) is good and, considering the wavelengths related to the dispersion curve frequency range, the V_S profile between 5 to about 100 metres is likely to be well constrained. Therefore, since below this depth the profile is constrained by the H/V curve alone, we prefer to show, in Figure 40**a** and Table 6, the V_S profile only within the depth range were both curves contribute to the inversion.

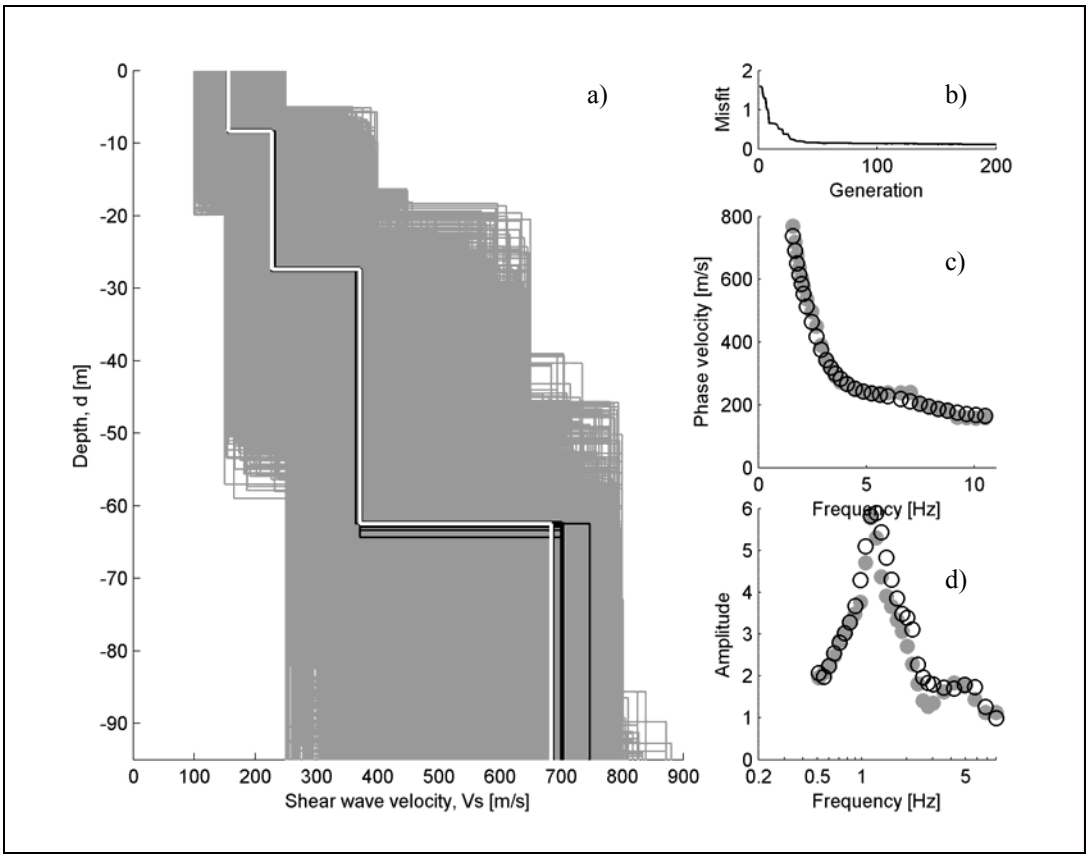

Figure 40 - Shear wave velocity model at the CTL station (a) and its fit to the dispersion (c) and H/V ratio curves (d). Fig. a: Tested models (grey lines), the minimum cost model (white line), and models lying inside the minimum cost + 10% range (black lines). b) The minimum misfit value versus generation. Fig. c-d: experimental (grey circles) and empirical – relevant to the minimum cost model – (white circles) values.

Shear wave velocity, V_S [m/s]	Thickness, h [m]
156	8.4
227	19.1
371	35.1
684	37.1

Table 6 Shear wave velocity model at the CTL station.

4.3.4. Comparison with independent data

The Emilia Romagna region has recently published on line a web-GIS[1] that allow accessing to the geologic maps (with different scales e.g. 1:50.000 to 1:10.000) of the whole region. Furthermore, also other types of data like borehole stratigraphies, SPT, shear wave velocity profile from Cross-Hole and Down-Hole tests, etc. are available. Figure 41 shows the 1:10000 geologic map of the study area, and the location of sites were Cross-Hole and Down-Hole tests were carried. Amongst all measurements nearby station CTL, only a Down-Hole test, evidenced in red, was performed in the same geologic formation (the Italian name reported in the web-GIS is "*Argille Azzurre*" and its litotechnic description is clay, silty-clay, and marly-clay). Figure 42 shows that the V_S profiles estimated at CTL and at the Down-Hole site are in a very good agreement (in the depth range they span in common) although the distance between the two sites is about 10 km.

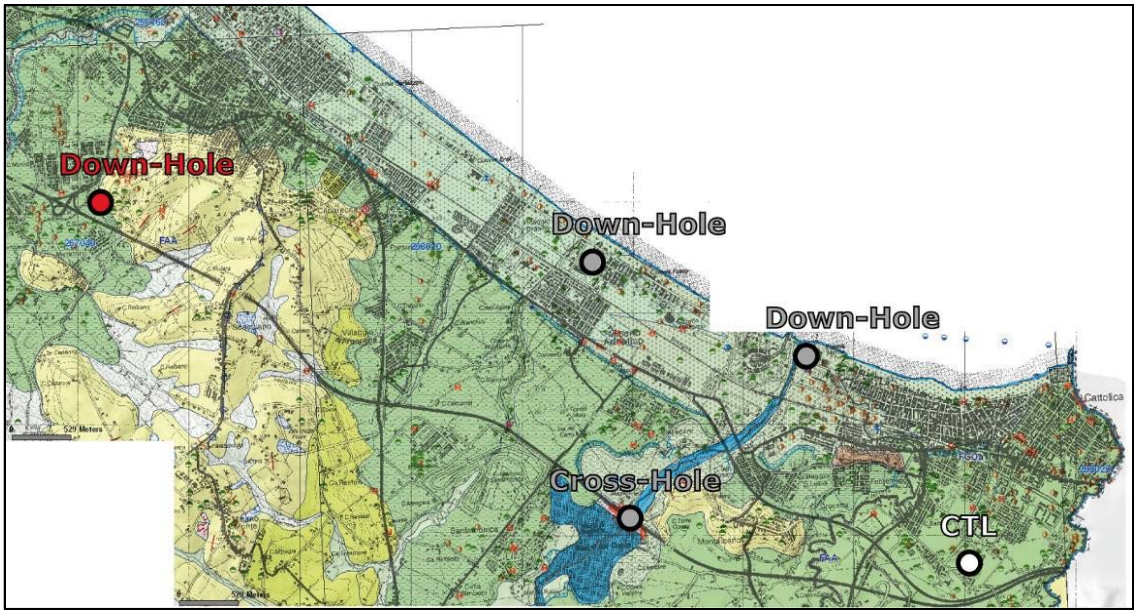

Figure 41 - 1:10.000 geologic map of the study area. The location of sites were Down- and Cross-Hole tests are available is indicated. The red circle highlight the location of the Down-Hole test performed shallow geology material similar to that existing at the CTL station.

1 http://geo.regione.emilia-romagna.it/carg/home.htm

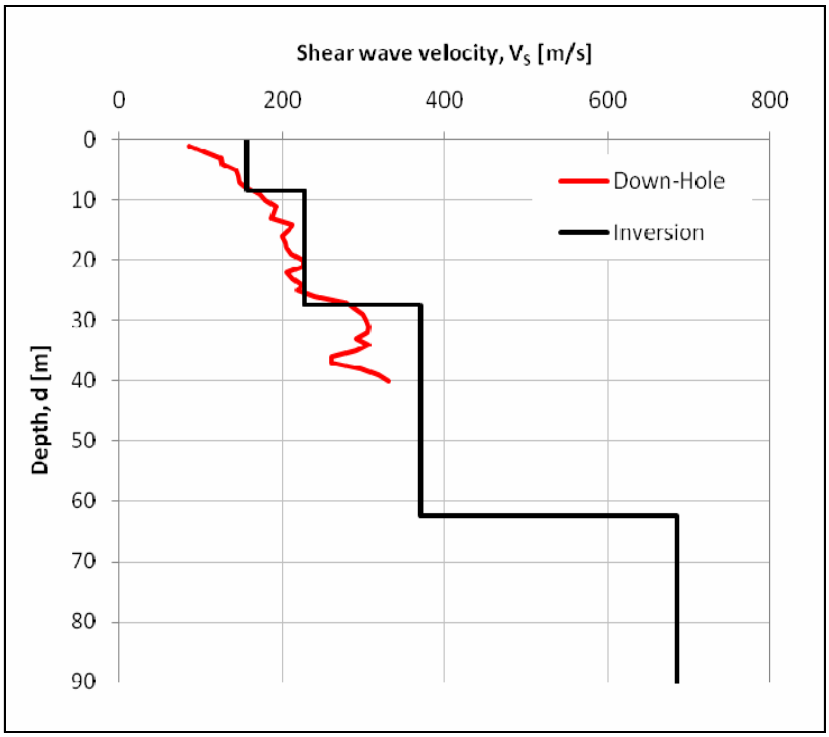

Figure 42 - Comparison between the Vs profile derived from the Down-Hole test data analysis (at a site 10 km faraway from the RAN station but on similar geological material) and by the joint inversion of dispersion and H/V curves.

4.4. UR7 –University of Siena

4.4.1. The Monte Cassino RAN site (MTC)

A first step, a detailed geologic survey of the area surrounding the RAN site was carried on.

The M. Cassino RAN station is located in the South-Eastern sector of Monte Cairo (Southern Latium). From a topographic point of view the M. Cassino RAN station belongs to the T4 topographic class.

The site is characterized by the cropping out of a thick Cretaceous inner platform succession belonging to the Laziale-abruzzse domain. The sedimentary succession is characterized by bioclastic limestones, brownish limestones, marls, bio-clastic calcarenites dolomitic limestones and dolomites. Field analyses carried out in the site allow us to identify up to 6 different formations as listed below: 6) Downward light brown micrite and bioclastic calcarenite with Orbitoidi, then mudstones/wackestones white and avana, with thin intercalations of clay and sporadic levels of flint. Middle portion is characterized by laminated dolomicrite and light brown mudstones/wackestones and marly-conglomeratic levels with large quantity of quartz. Upward dolomite with laminations and saccaroid dolomites. 5) Brownish mudstones/wackestones, dolomitic limestones, dolomites with rare siliceous levels. Thin clay-marly levels, reddish paleosoils. Conglomerates, reddish calcareous hard-ground and dark dolomites. 4)Bioturbated dolomitic limestones and mudstones/wackestones. In the upper part bioclastic crystalline calcarenites/calcurydites. 3) Mainly whitish mudstones/wackestones, with rare intercalations of bioclastic calcarenites/calcirudites; abundant bioclastic calcarenites/calcirudites; abundant biostromal levels and dissolution

processes. 2) Calcareniti a Briozoa member has been distinguished. Whitish/gray calcarenites/calcirudites with Briozoa and fragments of Lithotamnium, interbedded with whitish saccaroids calcarenites laterally passing to gray-yellowish calcarenites with Briozoa and Pecten. 1) Continental deposits mainly characterized by alluvial/colluvial deposits.

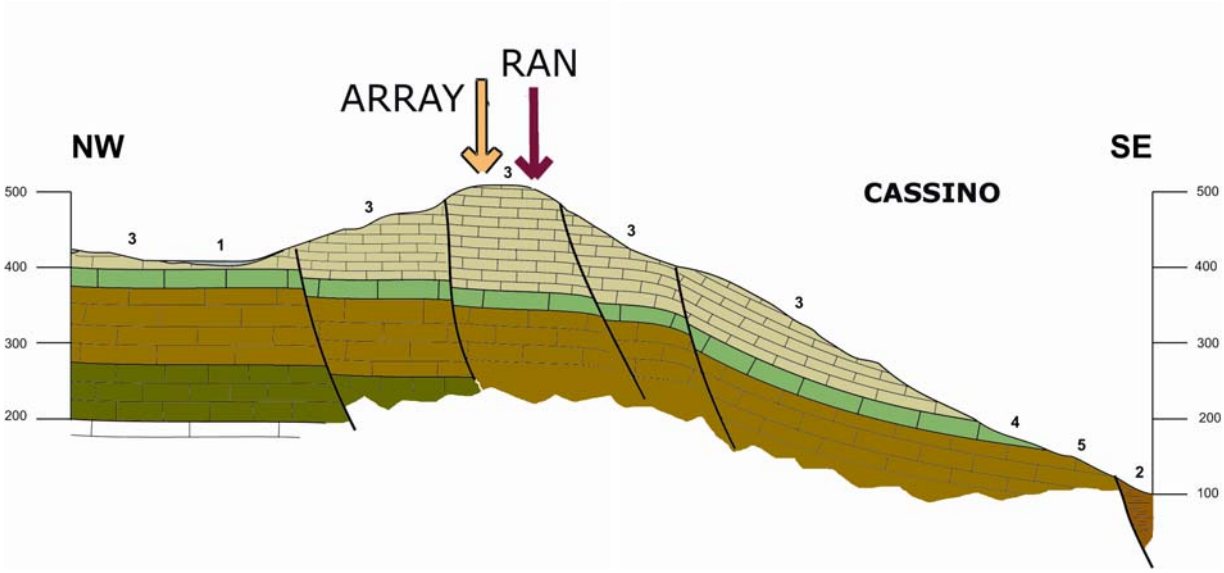

Figure 43 Geological section across Montecassino area: RAN indicates location of the MTC accelerometric station. ARRAY indicates the position of the array

The site is characterized by the presence of several faults. These last has been cinematically characterized as normal faults, mainly dip-slip, with an anti-apenninic SW-NE trend. The average deep angle is 70-80° SE that gradually offset toward the South-Eastern sector the whole sedimentary succession. An important normal fault N-S trending offset to the E the upper portion of the succession as demonstrated by the cropping out of the Miocene formation at the base of the M. Cassino hill.

A representative geological section is reported in Figure 43.

4.4.2. Passive seismic prospecting: Results

A single station measurement was carried nearby the RAN station (Figure 44) on 15 of May 2009. The analysis of this measurement revealed the presence of strong electromagnetic noise affecting a significant range of frequencies.

Figure 44. Location of the RAN station and of the corresponding single station ambient vibration measurement

The resulting HVSR curve is reported in Figure 45. One can see that, if one discards the apparent peak around 1-2 Hz induced by electromagnetic noise, a sharp peak only emerges in the high frequency range (just above 18 Hz) that can be attributed to a very thin soft coverage of the rock that constitutes the bulk of the hill.

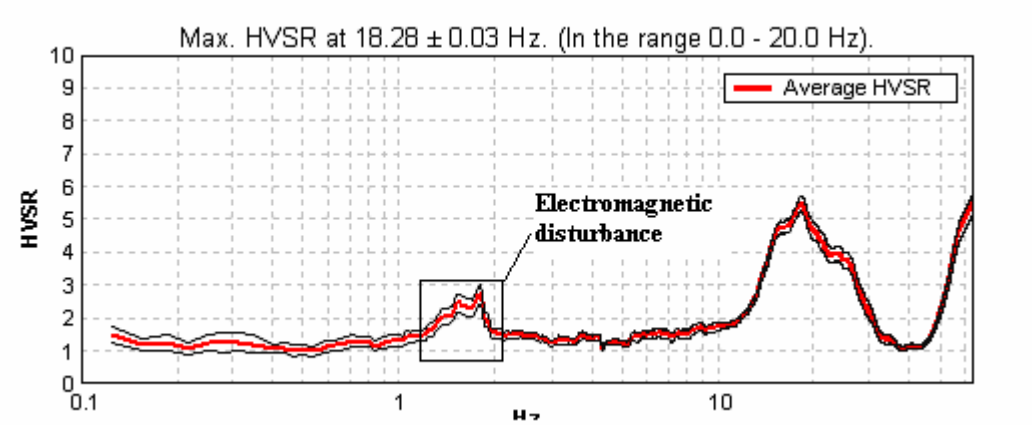

Figure 45. HVSR curve obtained at the RAN station. The red line indicates the average HVSR values, while the black thin lines indicate the relevant 95% confidence interval

Due to the very difficult topographic situation (the RAN station is located at the edge of the terrace where the Montecassino Abbay is located, Figure 46), array measurements were carried on at foothill, few hundreds meters apart.

The apparent VR pattern is shown in Figure 47. Geological analyses indicate that at the array, seismic bedrock is nearly outcropping. The shape of apparent VR values is compatible with a uniform rock formation characterised by a Vs value of the order of 1400 m/sec. At the site were array was located, a number of HVSR measurements were carried on the reveal possible lateral variations in the subsoil around the array. All the relevant HVSR curves resulted flat, confirming geological indications and suggesting that a uniform rock body constitutes the local subsoil.

Figure 46. Location of the RAN station, at the edge of the terrace where the Montecassino Abbay is located

However, uniform subsoil is incompatible with the HVSR curve at the RAN station, where a resonance frequency was detected by HVSR measurements, that is compatible with the presence of a sharp shallow transition between a soft coverage and the underlying seismic bedrock.

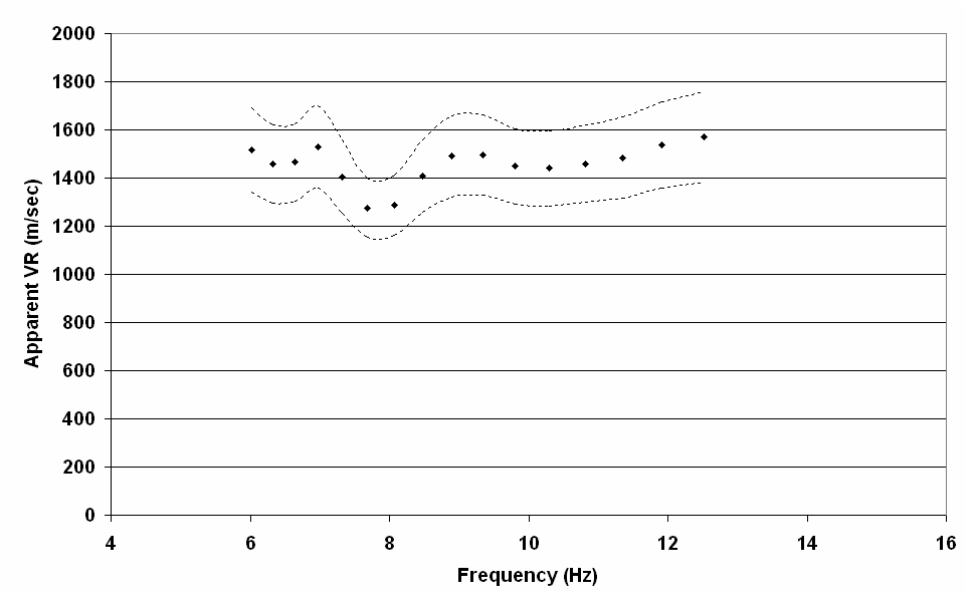

Figure 47. Apparent VR curve deduced from array measurements. Dots indicate VR estimates while dashed lines bound the relevant 95% confidence interval

In order to make these results compatible, an inversion of HVSR curve in Figure 47 was attempted by using Genetic Algorithms technique. In this inversion, Vs velocity of the seismic bedrock was kept fixed to the value deduced from array measurements and a soft coverage configuration was searched for, that is compatible with HVSR at the RAN station. Outcomes of this inversion are reported in Figure 48 where the presence of thin soft layer (about 5 m thick) is revealed above the seismic bedrock

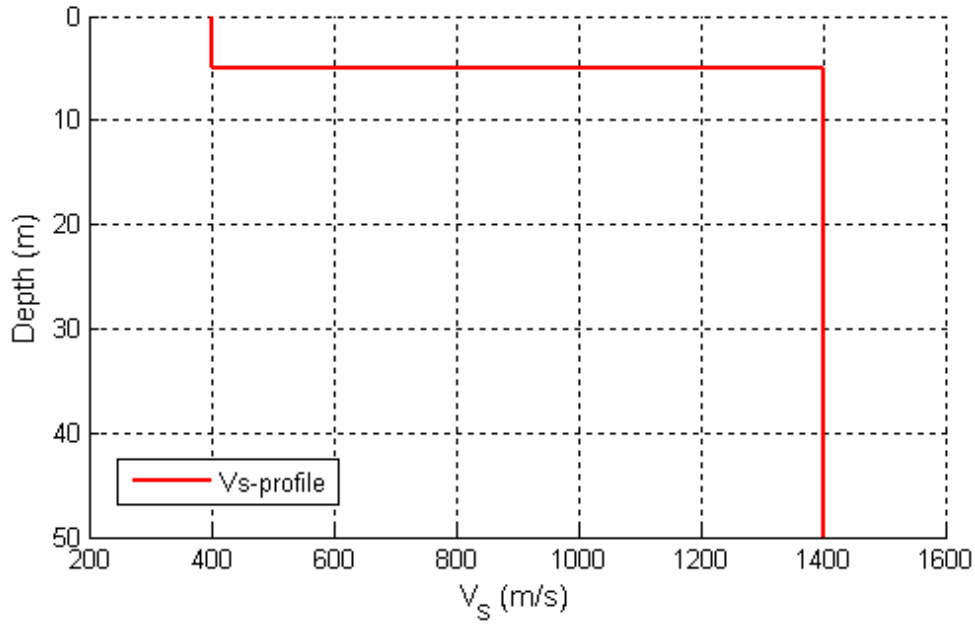

Figure 48. Vs Velocity profile at the Montecassino RAN station

5. Summary of results

In **Errore. L'origine riferimento non è stata trovata.** the results for the RAN stations investigated by each RU during S4 project are summarized.

Where the soil model obtained by the seismic tests does not reach 30 m depth, the $V_{S,30}$ is estimated using the correlation proposed by Figini (2006). For sites with shallow seismic bedrock also the seismic bedrock depth, the average Vs to the seismic bedrock and the natural frequency were calculated. The seismic bedrock is conventionally defined as V_S higher than 800 m/s. The average velocity is the inverse of the weighted average of the slownesses, and the natural frequency has been estimated as the ratio between the average velocity to the seismic bedrock and 4 times the seismic bedrock depth. For several stations, the natural frequency was also detrmined experimentally using the H/V spectral ratio method.

In the table also the type of surface wave method applied at each site is specified on the basis of the experimental protocol: A for active-source tests, i.e. MASW; P for passive-source methods, i.e. array measurements of microtremors. From the analysis of the results, we can observe that, with reference to the sites investigated in this project, RAN stations in Liguria, Piemonte and Sicilia are mainly shallow seismic bedrock sites and consequently they are characterized by a natural frequency around or greater than 10 Hz, whereas RAN stations in the Central of Italy are characterized by a natural frequency below 10 Hz, and often below 1Hz.

Table 7 Synthesis of the results

Site	Station	VS_{30} (m/s)	Bedrock (m)	VS_h (m/s)	f_0 (exp.) (Hz)	f_0 (Hz)	Test	RU
RONCO SCRIVIA	RNS	737					MASW	4
SESTRI LEVANTE	SEL	606					MASW	4
GENOVA	GNV	987	3	366		29	MASW	4
VARESE LIGURE	VRL	758	6	456		18	MASW	4
TORTONA	TRT	483	13	306		6	MASW	4
PINEROLO	PNR	383					MASW	4
FIUME ATERNO	AQA	495	26	449		4	MASW	4
GELA	GEL	245					MASW	4
CALTAGIRONE	CLG	373					MASW	4
PATTI (CAB. ENEL)	PTT0	251					MASW	4
TORRE FARO	TRF0	302					MASW	4
TORTORICI	TOR	525	18	368		5	MASW	4
ISPICA	ISI	1482	1	338		106	MASW	4
NOTO	NTE	710	8	384		13	MASW	4
RAGUSA	RGS	1091	2	297		37	MASW	4
SANTA CROCE	SCR	894	4	299		20	MASW	4
CATANIA - PIANA	CAT	160					MASW	4
PALAZZOLO	PLZ	670	7	308		11	MASW	4
PACHINO	PCH	593	15	460		8	MASW	4
GEMONA	GMN	445					MASW	4
LA SALLE 2	LSA2	684					DH	4
LA SALLE 4	LSA4	540					DH	4
TORRE PELLICE 4	PE4	1048	3	366		29	DH	4
TORRE PELLICE 7	PE7	856	6	456		18	DH	4
BEVAGNA	BVG	170			1.22	1.72	ESAC/FK	8
NORCIA ZONA	NRZI	557	146	559	0.72	0.95	ESAC/FK	8
GRUMENTO NOVA	GRM	283			0.59	0.92	ESAC/FK	8
SANT ARCANGELO	SNA	420			0.34	1.03	ESAC/FK	8
LAGONEGRO	LGN	451	88	619		4.75	ESAC/FK	8
BAZZANO	BZZ	679	22	640			ESAC/FK	8
ONNA	ONNA	378			2.50		ESAC/FK	8
CATTOLICA	CTL	208			1.16	1.40	ESAC/FK	8
ARGENTA	ARG	170			0.34	0.34	ESAC/FK	8
FAENZA	FAZ	293				0.38	ESAC/FK	8
MODENA	MDN	213			0.65	0.75	ESAC/FK	8
NOVELLARA	NVL	190			0.65	0.66	ESAC/FK	8
ASSERGI	GSA	488	40	531	4.5	5	MASW	2
AVEZZANO	AVZ	199	160	390	0.8	0.7	MASW	2
BIBBIENA NUOVA	BBN	1000-1200			No peak		MASW	2
BORGO OTTOMILA	BTT2	92	300	250	0.3	0.3	MASW	2
CASSINO	CSS	630	?	?	2.5-3.5	2.5-	MASW	2
DICOMANO	DCM	1000			20-25		MASW	2
RIETI	RTI	170	200	390	0.8	0.7	MASW	2
CAPESTRANO	CPS	730	19	630	2.7		ESAC/HV	7
AQUILA COLLE DEI	AQG	1150	0	0	6.3		ESAC/HV	7
PESCASSEROLI	PSC	1000	0	0	4.3		ESAC/HV	7
AQUILA PETTINO	AQP	830	7	500	1.9		ESAC/HV	7
SCANNO	SCN	840	20	750	3.6		ESAC/HV	7
MORMANNO	MRM	1400	0	0	No		ESAC/HV	7
SPEZZANO SILA	SPS	320	29	310	3.4		ESAC/HV	7
VIBO MARINA	VBM	450	34	460	5.2		ESAC/HV	7
VIBO VALENTIA	VBV	510	24	450	13.5		ESAC/HV	7
MONTECASSINO	MTC	1000	5	400	18.3		ESAC/HV	7
MARSICO VETERE	MRV	680	17	590	7		ESAC/HV	7
PIGNOLA	PGA	430	20	340	5.6		ESAC/HV	7
SATRIANO	STL	390	53	530	No		ESAC/HV	7
TRICARICO	TRO	780	0	0	No		ESAC/HV	7
AQUILA F. ATERNO	AQA	552					DH	6
AQUILA C GRILLI	AQG	685					DH	6

Site	Station	VS_{30} (m/s)	Bedrock (m)	VS_h (m/s)	f_0 (exp.) (Hz)	f_0 (Hz)	Test	RU
AQUILPARK	AQK	717					DH	6

References

Aki, K., 1957. Space and Time Spectra of Stationary Stochastic Waves, with Special Reference to Microtremors, *Bull. Earthq. Res. Inst. Tokyo*, 35, 415-457.

Arai H. and K. Tokimatsu, 2004. S-wave velocity profiling by inversion of microtremor H/V spectrum, Bull. Seism. Soc. Am., 94, 53–63.

Bergamo P., Comina C., Foti S., and Maraschini M., Seismic characterization of shallow bedrock sites with surface wave analysis, Submitted to Soil Dynamics and Earthquake Engineering.

Bettig B., Bard P.Y., Scherbaum F., Riepl J. , Cotton F. , Cornou C. and D. Hatzfeld, 2001. Analysis of dense array measurements using the modified spatial auto-correlation method (SPAC). Application to Grenoble area, *Bollettino di Geofisica Teorica e Applicata*, 42, 3-4, 281-304.

Capon, J., 1969. High-Resolution Frequency-Wavenumber Spectrum Analysis, *Proceedings of the IEEE*, 57, No. 8, 1408-1419.

Comina C., Foti S., Boiero D. and Socco L.V., 2010, Reliability of vs,30 evaluation from surface waves tests, Journal of Geotechnical and Geoenvironmental Engineering, ASCE, submitted

Deliverable 6, 2009. Responsibles: Pacor F. and Paolucci R.; edited by: Foti S., Parolai S. and Albarello D.; contributors: Albarello D., Comina C., Foti S., Maraschini M., Parolai S., Picozzi M., Puglia R. and Tokeshi K.; Research Report of DPC-INGV S4 Project 2007-2009. http://esse4.mi.ingv.it

Douze, E. J. and S.J. Laster, 1979. Statistics of semblance, *Geophysics*, 44, 1999–2003.

Figini R, 2006. Analisi degli effetti di sito sui lunghi periodi degli spettri di risposta di spostamento. Master's Thesis, Politecnico di Milano (in Italian).

Foti S., Comina C., Boiero D., Socco L.V. . 2009. Non uniqueness in surface wave inversion and consequences on seismic site response analyses, Soil Dynamics and Earthquake Engineering, Vol. 29 (6), 982-993.

Haskell, N., 1964, Radiation pattern of surface waves from point sources in a multilayered medium: Bulletin of seismological society of America, 54, no. 1, 377-393.

Herrmann R.B., Ammon C.J., Julia J. and Mokhtar T., 1999. Joint inversion of receiver functions and surface-wave dispersion for crustal structure. Proc. 21st Seismic Research Symposium Technologies for monitoring the comprehensive Nuclear test Ban treaty, September 21-24, 1999, Las Vegas, Nevada, USA, published by Los Alamos National Laboratory, LA-UR-99-4700.

Herrmann, R. B., and C. Y. Wang, 1980, A numerical study of p-, sv- and sh- wave generation in a plane layered medium: Bulletin of seismological society of America, 70, no. 4, 1015-1036.

Herrmann, R. B., 2002, SURF code, www.eas.slu.edu/People/RBHerrmann/.

Horike, M., 1985. Inversion of phase velocity of long-period microtremors to the S-wave-velocity structure down to the basement in urbanized areas, *J. Phys. Earth.* 33, 59–96.

Kitsunezaki C., Goto N., Kobayashi Y., Ikawa T., Horike M., Saito T., Kurota T., Yamane K. and Okozumi K., 1990. Estimation of P- and S-wave velocities in deep soil deposits for evaluating ground vibrations in earthquake. J.JSNDS, 9, 1-17.

Konno K. and Ohmachi T., 1998. Ground-Motion Characteristics Estimated from Spectral Ratio between Horizontal and Vertical Components of Microtremor, Bull. Seism. Soc. Am., 88, 228-241.

Lacoss R.T., Kelly E.J., Toksöz M.N., 1969. Estimation of seismic noise structure using arrays, Geophysics, 34, 21-38.

Louie, J., 2001. Faster, Better: Shear-Wave Velocity to 100 Meters Depth from Refraction Microtremor Arrays, *Bull. Seism. Soc. Am*, 91, 347 - 364.

Lunedei E., Albarello D. (2009). On the seismic noise wavefield in a weakly dissipative layered Earth. *Geophysics. J. Int.* (2009) **177,** 1001–1014, doi: 10.1111/j.1365-246X.2008.04062.x

Maraschini, M., F. Ernst, S. Foti, and L.V. Socco, 2010, A new misfit function for multimodal inversion of surface waves. Geophysics, in print.

Maraschini, M. and S. Foti, 2010, A Monte Carlo multimodal inversion of surface waves: Geophysical Journal International, in print.

Neiddell, N. and M. T. Taner, 1971. Semblance and other coherency measures for multichannel data, *Geophysics*, 36, 482–497.

Ohori M., Nobata A., and Wakamatsu K., 2002. A comparison of ESAC and FK methods of estimating phase velocity using arbitrarily shaped microtremor analysis, Bull. Seism. Soc. Am., 92, 2323-2332.

Okada, H. (2003). The microtremor survey method, *Geophysics. Monograph Series,* Vol. 12, Society of Exploration Geophysicists, 129 pp.

Parolai S., Mucciarelli M., Gallipoli M.R., Richwalski S.M. and Strollo A., 2007. Comparison of Empirical and Numerical Site Responses at the Tito Test Site, Southern Italy, Bull. Seism. Soc. Am., 97, 1413-1431.

Parolai S., Picozzi M., Richwalski S.M. and Milkereit C., 2005. Joint inversion of phase velocity dispersion and H/V ratio curves from seismic noise recordings using a genetic algorithm, considering higher modes, Geoph. Res. Lett., 32, doi: 10.1029/2004GL021115.

Parolai S., Richwalski S.M., Milkereit C. and Faeh D., 2006. S-wave velocity profile for earthquake engineering purposes for the Cologne area (Germany), Bull. Earthq. Eng., 65–94, doi:10.1007/s10518-005-5758-2.

Picozzi M., Parolai S., Albarello D.; 2005: Statistical analysis of noise Horizonatal-to-Vertical Spectral Ratios (HVSR). Bull. Seism. Soc. Am., **95**, n. 5, 1779–1786, doi: 10.1785/0120040152

Picozzi M., Albarello D. (2007). Combining genetic and linearized algorithms for a two-step joint inversion of Rayleigh wave dispersion and *H/V* spectral ratio curves. *Geophys. J. Int.* (2007) **169,** 189–200, doi: 10.1111/j.1365-246X.2006.03282.x

Sambridge, M., 1999. Geophysical inversion with a neighborhood algorithm: I. Searching a parameter space, *Geophys. J. Int*. 138, 479– 494.

SESAME; 2004: Guidelines for the implementation of the H/V spectral ratio technique on ambient vibrations. SESAME, European project, WP12, Deliverable D23.12, http://sesame-fp5.obs.ujfgrenoble.fr/SES TechnicalDoc.htm

Thomson, W. T, 1950., Transmission of elastic waves through a stratified solid medium: Journal of Applied Physics, 21, no. 89.

Thorson, J. R., and J. F. Claerbout, 1985. Velocity-stack and slant-stack stochastic inversion, *Geophysics* 50, 2727–2741.

Tokimatsu K., Tamura S. and Kojima H., 1992. Effects of multiple modes on Rayleigh wave dispersion characteristics. Journal of Geotechnical Engineering 118, 1529–1543.

Tokimatsu, K. (1997). “Geotechnical Site Characterization using Surface Waves.” *Proceedings, First International Conference on Earthquake Geotechnical Engineering, IS-Tokyo '95*, Tokyo, November 14-16, Balkema, Rotterdam, 1333-1368.

Wang R., 1999. A simple orthonormalization method for stable and efficient computation of Green’s functions. Bulletin of the Seismological Society of America 89, 733–741.

Wathelet, M., 2008. An improved neighborhood algorithm: parameter conditions and dynamic scaling, *Geophys. Res. Lett.* 35.

Yamanaka H. and Ishida H., 1996. Application of Generic algorithms to an inversion of surface-wave dispersion data. Bull. Seism. Soc. Am. 86, 436-444.

Zhang, S.H., Chan, L.S. and Xia, J. (2004). The selection of field acquisition parameters for dispersion images from multichannel surface wave data. *Pure and Applied Geophysics* 161, 185–201.

Addendum: proposal for a reliability classification of *HVSR measurements*

Goal of this classification is providing a direct indication about the reliability of a single HVSr measurement, aiming at supporting operators during interpretation phase, when data provided by various groups and obtained in different conditions are compared. Criteria here proposed are more stringent than those proposed in the frame of the SESAME project since they take into account a larger set of criteria, that include the ones proposed by SESAME. In particular, the following features are taken into account:

The overall duration of the measurement

Time stationary character of H/V spectral ratios estimates

Isotropy of measured H/V spectral ratios estimates

Absence of electromagnetic disturbance

The overall shape of the HVSR curve

The comparison is generally performed on HVSR measurements deduced from average spectra smoothed with a triangular moving window with a spectral amplitude equal to 5% of the central frequency. Larger windows can be considered in some cases when this choice significantly improves readability of the HVSR curve.

Three quality classes are proposed. The meaning of each class and criteria adopted to attribute measurements to each class are reported below

Class A*: Reliable and physically plausible* HVSR curve, that can be interpreted by alone

The shape of the HVSR curve in the frequency range of concern is stationary for at least 30% of the measurement duration (*Stationary HVSR curve*)

Azimuthal variations in the HVSR amplitudes at the maxima do not exceeded 30% of the relevant maximum (*Isotropy*)

No trace of electromagnetic noise of anthropic origin present in the frequency range of interest (*Absence of disturbance*)

HVSR maxima are the result of a localized reduction of the vertical amplitude of ambient vibration spectral amplitudes (*Physical plausibility*)

SESAME criteria for a reliable HVSR curve are satisfied (*Statistical Robustness*)

Measurement duration is at least 15/20 minutes (*Duration*)

Class B*: suspect* HVSR curve (to be "interpreted"): it can be considered with caution and only when coherent with other measurements carried on nearby

1. At least one of the conditions of class A is not satisfied

Class C*: bad* HVSR curve: it should be discarded

B type measurement in the presence of drift increasing towards lower frequencies, possible effect of instrument movements during the measure

B type measurement where electromagnetic disturbances affect several parts of the curve in the frequency range of interest

The above criteria do not concern the Interpretation of the curve in terms of subsoil configuration: in this case, further criteria are necessary (e.g., SESAME criteria for a “clear” peak. To this purpose, two sub classes are added:

Type 1. HVSR curve presents at least one “clear” peak by following the SESAME criteria (*a possible resonance is detected)*

Type 2. HVSR curve does not present any clear peak in the frequency range of interest (*no resonance*)

Some application examples are reported below

Example 1

Class B1 (Does not satisfy isotropy condition but it presents a very clear peak)

Trace length: 0h20'00". Analysis performed on the entire trace.

Sampling frequency: 128 Hz

Window size: 30 s

Smoothing window: Triangular window

Smoothing: 5%

HORIZONTAL TO VERTICAL SPECTRAL RATIO

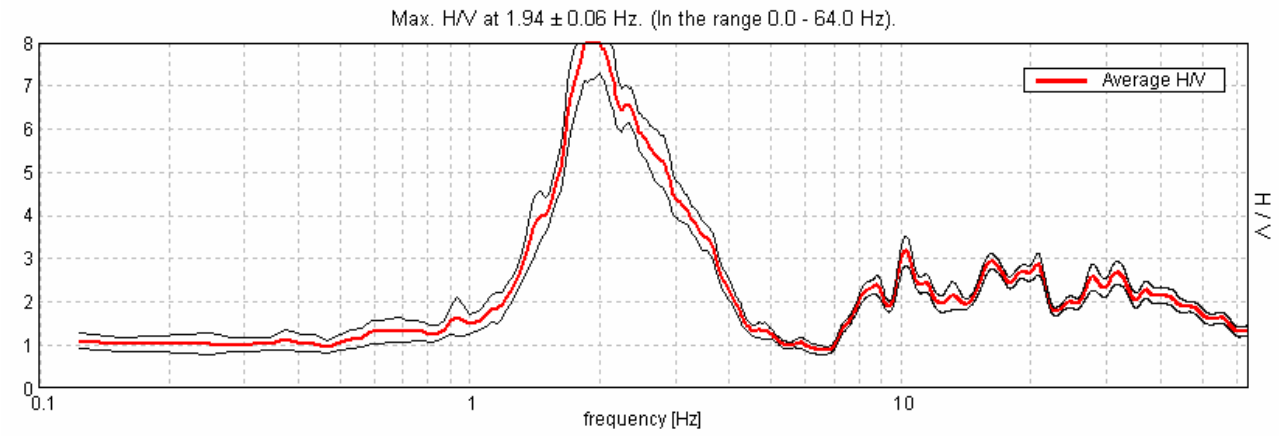

H/V TIME HISTORY

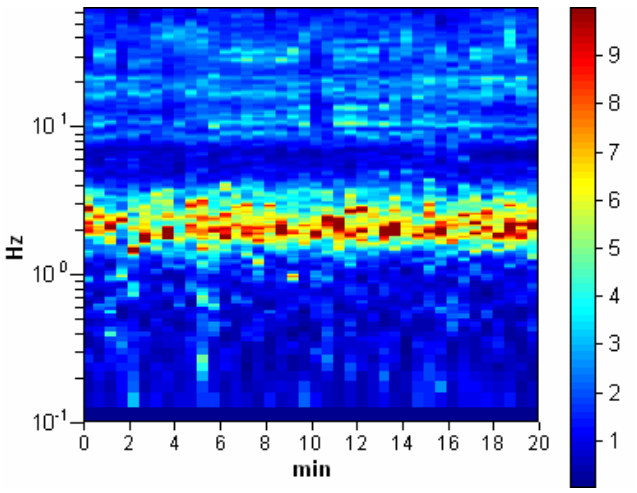

DIRECTIONAL H/V

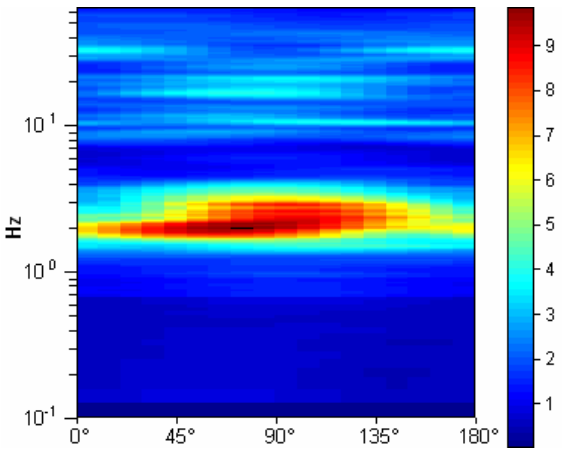

SINGLE COMPONENT SPECTRA

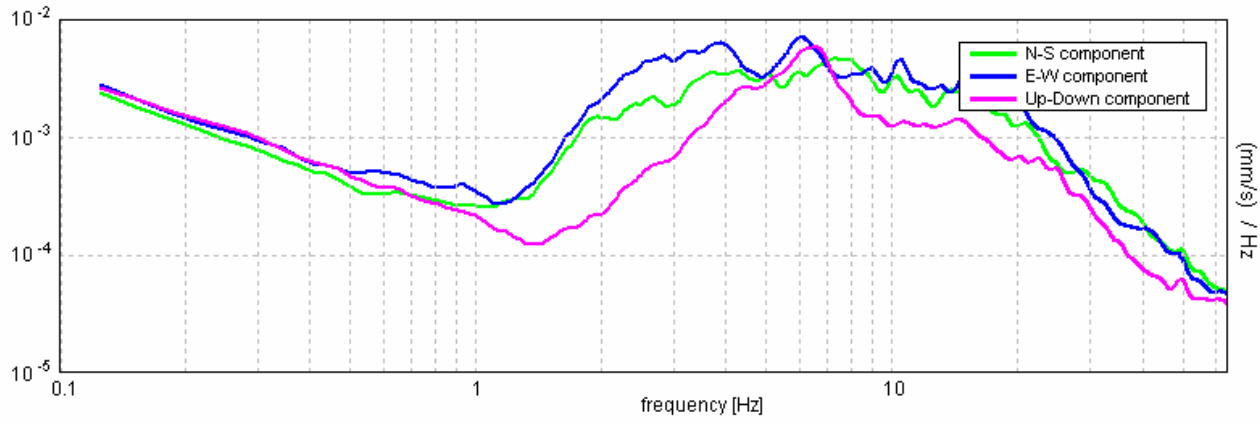

Max. H/V at 1.94 ± 0.06 Hz. (in the range 0.0 - 64.0 Hz).

Criteria for a reliable HVSR curve

[All 3 should be fulfilled]

$f_0 > 10 / L_w$	1.94 > 0.33	**OK**	
$n_c(f_0) > 200$	2325.0 > 200	**OK**	
$\sigma_A(f) < 2$ for $0.5f_0 < f < 2f_0$ if $f_0 > 0.5$Hz **$\sigma_A(f) < 3$ for $0.5f_0 < f < 2f_0$ if $f_0 < 0.5$Hz**	Exceeded 0 out of 94 times	**OK**	

Criteria for a clear HVSR peak

[At least 5 out of 6 should be fulfilled]

Exists f^- in $[f_0/4, f_0]$ | $A_{H/V}(f^-) < A_0 / 2$	1.5 Hz	**OK**	
Exists f^+ in $[f_0, 4f_0]$ | $A_{H/V}(f^+) < A_0 / 2$	3.25 Hz	**OK**	
$A_0 > 2$	8.03 > 2	**OK**	
$f_{peak}[A_{H/V}(f) \pm \sigma_A(f)] = f_0 \pm 5\%$	|0.01558| < 0.05	**OK**	
$\sigma_f < \varepsilon(f_0)$	0.03019 < 0.19375	**OK**	
$\sigma_A(f_0) < \theta(f_0)$	0.4295 < 1.78	**OK**	

Example 2:

Class A1 (azimuthal variations do not exceed 30% of the maximum value and at least one clear peak is identified)

Trace length: 0h20'00". Analysis performed on the entire trace.

Sampling frequency: 128 Hz

Window size: 30 s

Smoothing window: Triangular window

Smoothing: 5%

HORIZONTAL TO VERTICAL SPECTRAL RATIO

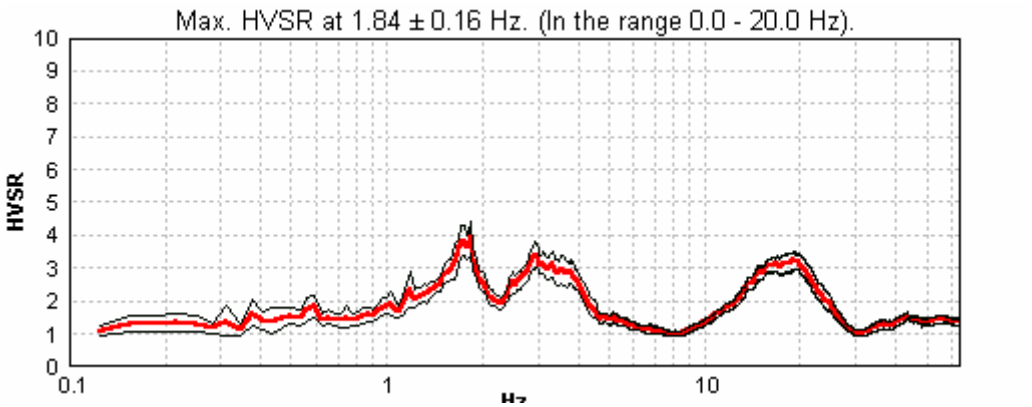

H/V TIME HISTORY

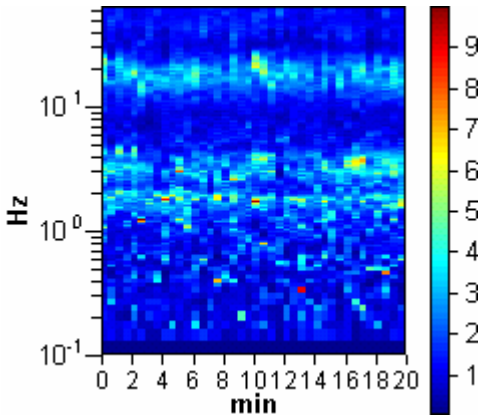

DIRECTIONAL H/V

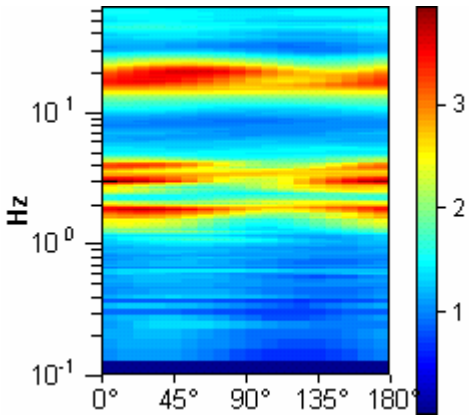

SINGLE COMPONENT SPECTRA

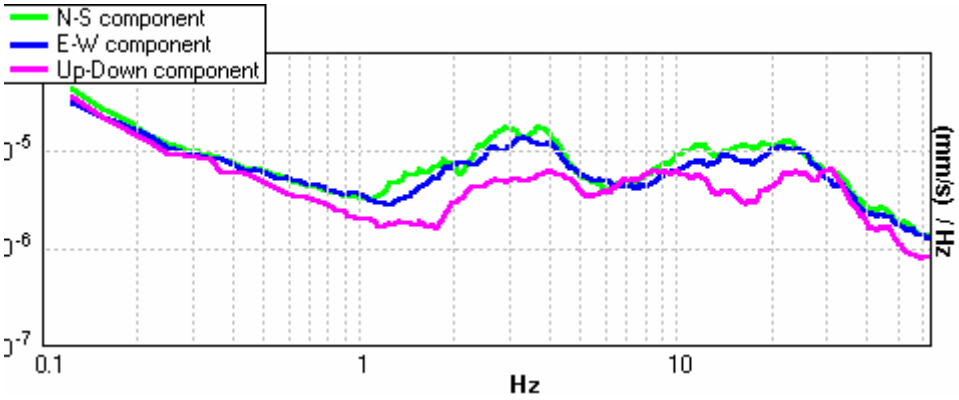

Max. HVSR at 1.84 ± 0.16 Hz. (in the range 0.0 - 20.0 Hz).

Criteria for a reliable HVSR curve

[All 3 should be fulfilled]

$f_0 > 10 / L_w$	1.84 > 0.33	OK	
$n_c(f_0) > 200$	2212.5 > 200	**OK**	
$\sigma_A(f) < 2$ for $0.5f_0 < f < 2f_0$ if $f_0 > 0.5$Hz **$\sigma_A(f) < 3$ for $0.5f_0 < f < 2f_0$ if $f_0 < 0.5$Hz**	Exceeded 0 out of 90 times	**OK**	

Criteria for a clear HVSR peak

[At least 5 out of 6 should be fulfilled]

Exists f^- in $[f_0/4, f_0]$ | $A_{H/V}(f^-) < A_0 / 2$	1.125 Hz	**OK**	
Exists f^+ in $[f_0, 4f_0]$ | $A_{H/V}(f^+) < A_0 / 2$	2.25 Hz	**OK**	
$A_0 > 2$	3.92 > 2	**OK**	
$f_{peak}[A_{H/V}(f) \pm \sigma_A(f)] = f_0 \pm 5\%$	|0.04173| < 0.05	**OK**	
$\sigma_f < \varepsilon(f_0)$	0.07693 < 0.18438	**OK**	
$\sigma_A(f_0) < \theta(f_0)$	0.2365 < 1.78	**OK**	

Example 3

Class B2: Strong directionality and possible presence of electromagnetic disturbance (below 20 Hz) in the lack of clear peaks

Trace length: 0h20'00". Analysis performed on the entire trace.

Sampling frequency: 128 Hz

Window size: 30 s

Smoothing window: Triangular window

Smoothing: 5%

HORIZONTAL TO VERTICAL SPECTRAL RATIO

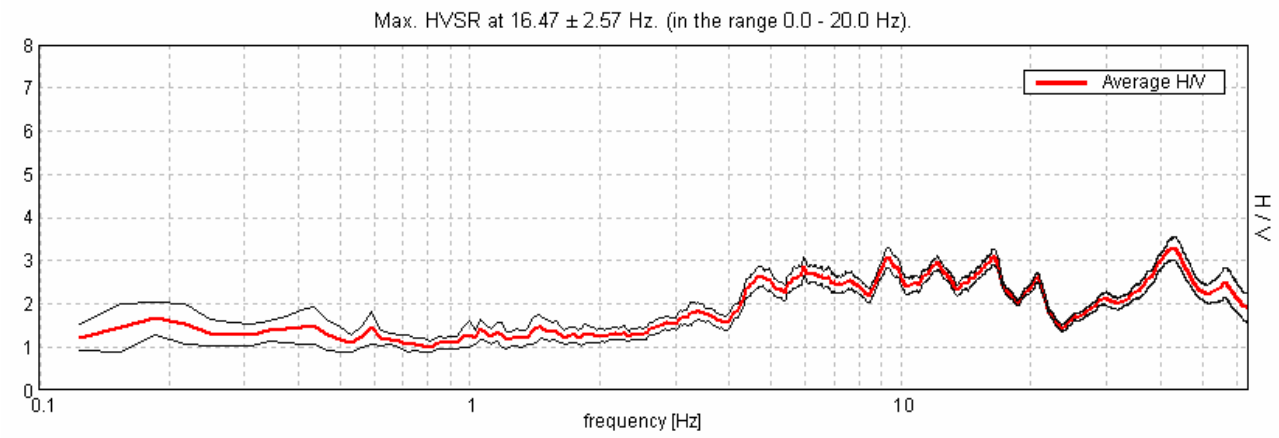

H/V TIME HISTORY

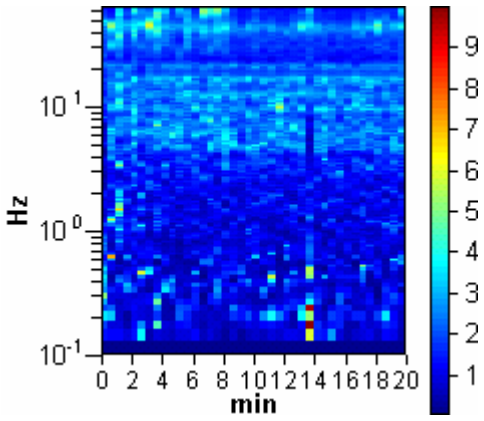

DIRECTIONAL H/V

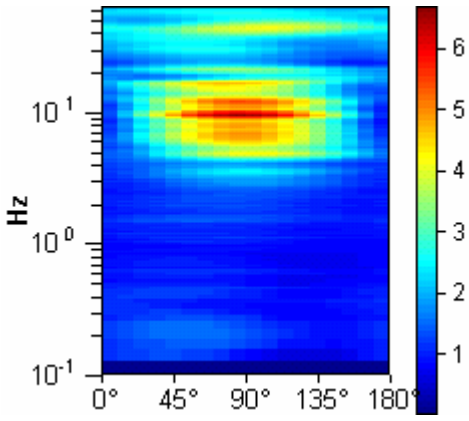

SINGLE COMPONENT SPECTRA

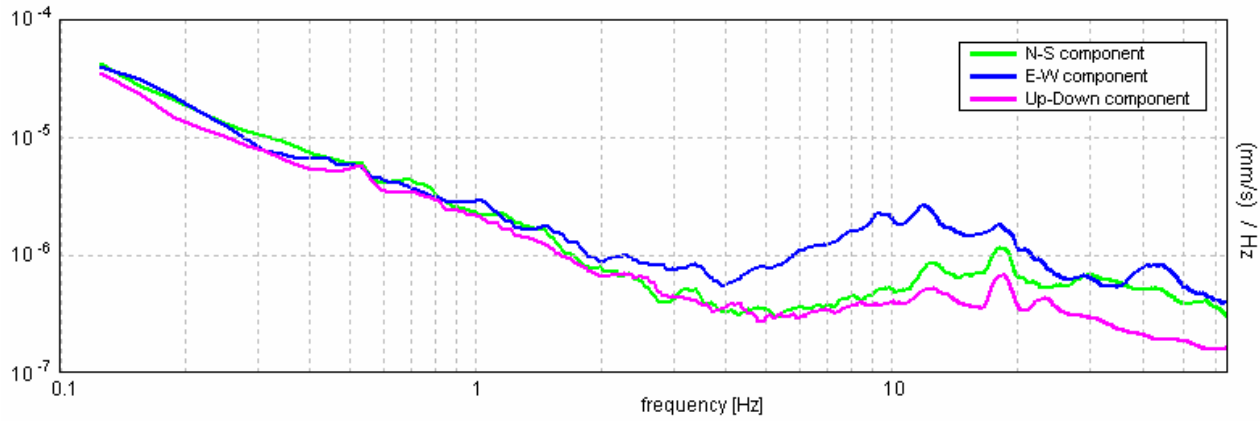

Max. HVSR at 16.47 ± 2.57 Hz. (in the range 0.0 - 20.0 Hz).

Criteria for a reliable HVSR curve [All 3 should be fulfilled]			
$f_0 > 10 / L_w$	16.47 > 0.33	OK	
$n_c(f_0) > 200$	19762.5 > 200	**OK**	
$\sigma_A(f) < 2$ for $0.5f_0 < f < 2f_0$ if $f_0 > 0.5$Hz **$\sigma_A(f) < 3$ for $0.5f_0 < f < 2f_0$ if $f_0 < 0.5$Hz**	Exceeded 0 out of 792 times	**OK**	
Criteria for a clear HVSR peak [At least 5 out of 6 should be fulfilled]			
Exists f^- in $[f_0/4, f_0]$ | $A_{H/V}(f^-) < A_0 / 2$			**NO**
Exists f^+ in $[f_0, 4f_0]$ | $A_{H/V}(f^+) < A_0 / 2$	23.063 Hz	**OK**	
$A_0 > 2$	3.08 > 2	**OK**	
$f_{peak}[A_{H/V}(f) \pm \sigma_A(f)] = f_0 \pm 5\%$	|0.07625| < 0.05		**NO**
$\sigma_f < \varepsilon(f_0)$	1.25582 < 0.82344		**NO**
$\sigma_A(f_0) < \theta(f_0)$	0.0882 < 1.58	**OK**	

Example 4

Class C2: Strong and widespread electromagnetic disturbance

Trace length: 0h20'00". Analysis performed on the entire trace.

Sampling frequency: 128 Hz

Window size: 20 s

Smoothing window: Triangular window

Smoothing: 5%

HORIZONTAL TO VERTICAL SPECTRAL RATIO

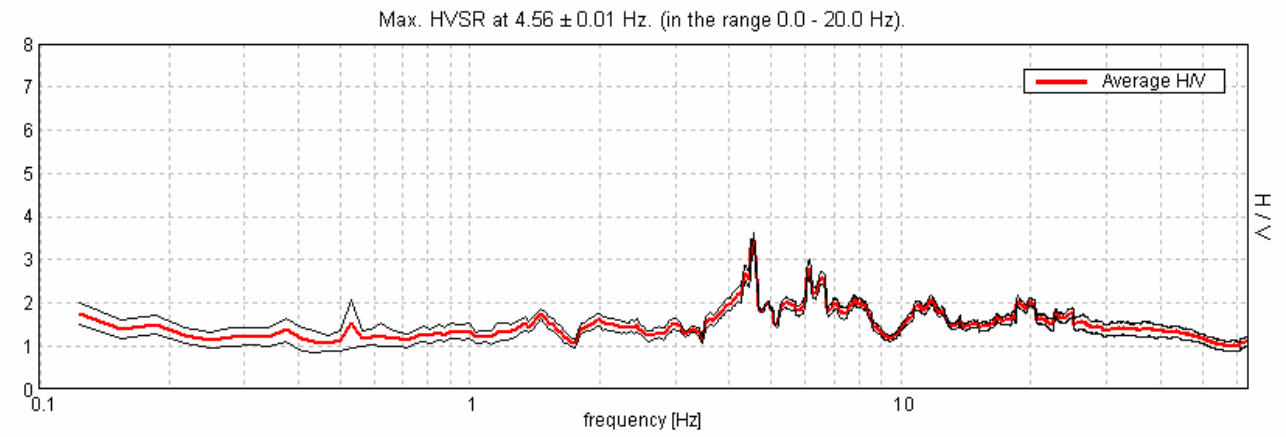

H/V TIME HISTORY

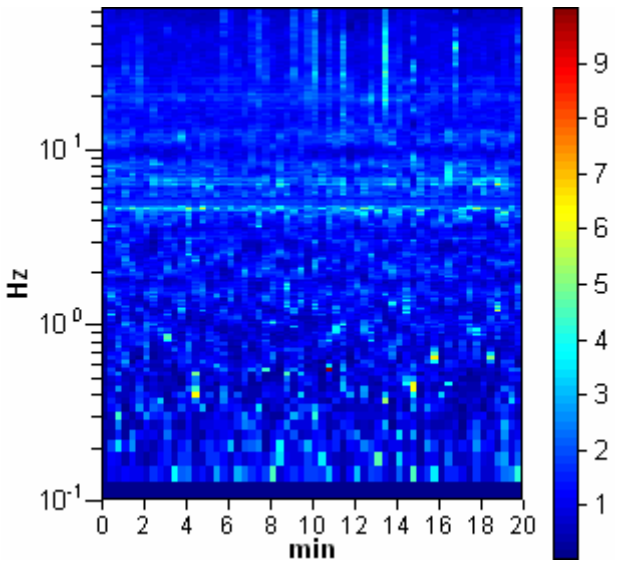

DIRECTIONAL H/V

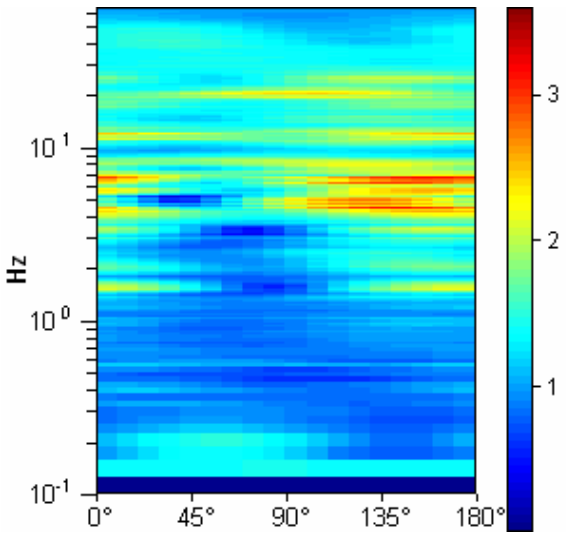

SINGLE COMPONENT SPECTRA

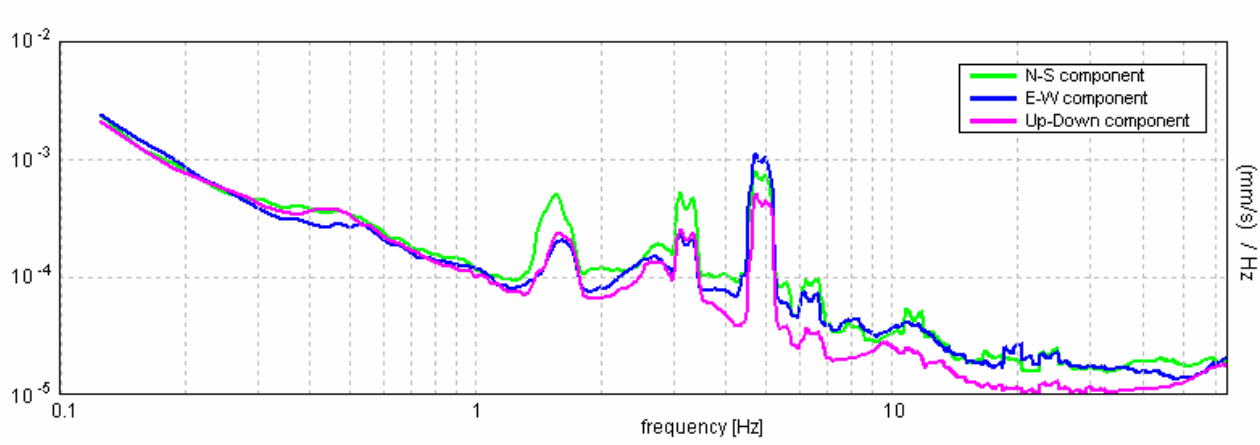

Max. HVSR at 4.56 ± 0.01 Hz. (in the range 0.0 - 20.0 Hz).

Criteria for a reliable HVSR curve

[All 3 should be fulfilled]

$f_0 > 10 / L_w$	4.56 > 0.50	OK	
$n_c(f_0) > 200$	5475.0 > 200	**OK**	
$\sigma_A(f) < 2$ for $0.5f_0 < f < 2f_0$ if $f_0 > 0.5$Hz **$\sigma_A(f) < 3$ for $0.5f_0 < f < 2f_0$ if $f_0 < 0.5$Hz**	Exceeded 0 out of 220 times	**OK**	

Criteria for a clear HVSR peak

[At least 5 out of 6 should be fulfilled]

Exists f^- in $[f_0/4, f_0] \mid A_{H/V}(f^-) < A_0 / 2$	3.781 Hz	**OK**	
Exists f^+ in $[f_0, 4f_0] \mid A_{H/V}(f^+) < A_0 / 2$	5.063 Hz	**OK**	
$A_0 > 2$	3.47 > 2	**OK**	
$f_{peak}[A_{H/V}(f) \pm \sigma_A(f)] = f_0 \pm 5\%$	|0.00066| < 0.05	**OK**	
$\sigma_f < \varepsilon(f_0)$	0.00299 < 0.22813	**OK**	
$\sigma_A(f_0) < \theta(f_0)$	0.0805 < 1.58	**OK**	

Example 5

Class B1: directionality in the presence of electromagnetic disturbance. A cleat HVSR peak is detected

Trace length: 0h20'00". Analysis performed on the entire trace.

Sampling frequency: 128 Hz

Window size: 30 s

Smoothing window: Triangular window

Smoothing: 5%

HORIZONTAL TO VERTICAL SPECTRAL RATIO

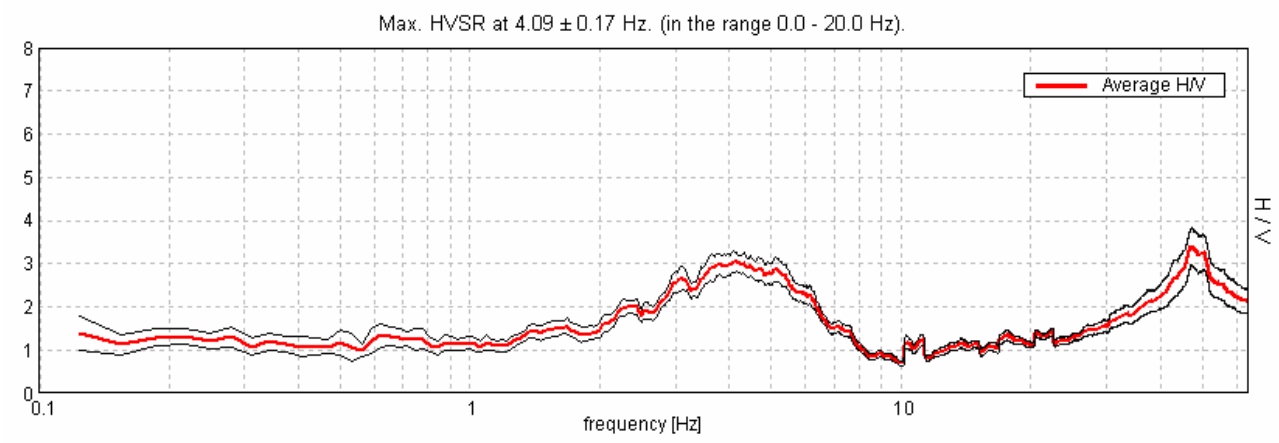

H/V TIME HISTORY

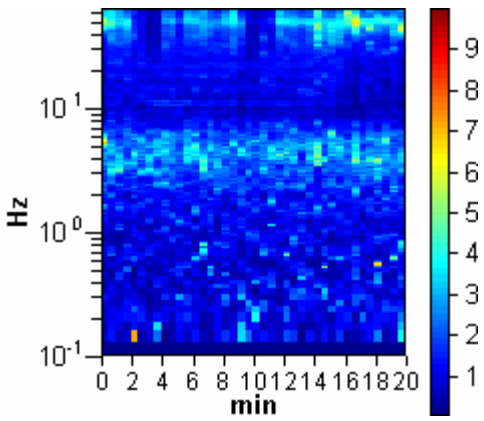

DIRECTIONAL H/V

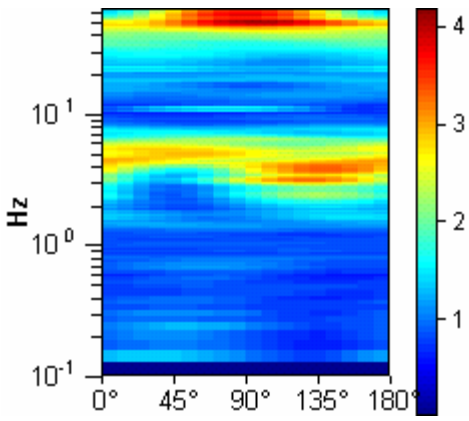

SINGLE COMPONENT SPECTRA

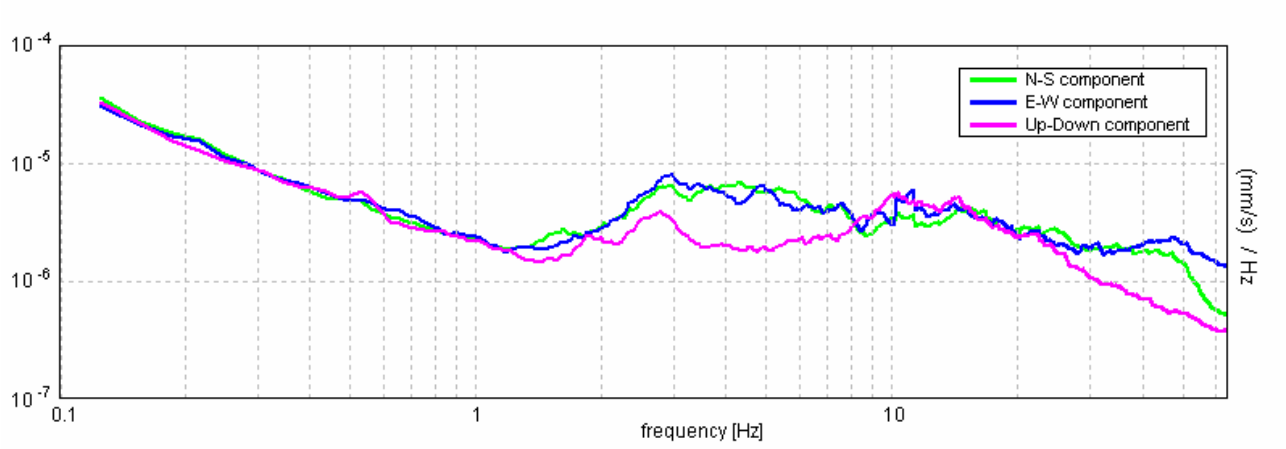

Max. HVSR at 4.09 ± 0.17 Hz. (in the range 0.0 - 20.0 Hz).

Criteria for a reliable HVSR curve [All 3 should be fulfilled]			
$f_0 > 10 / L_w$	4.09 > 0.33	OK	
$n_c(f_0) > 200$	4912.5 > 200	**OK**	
$_A(f) < 2$ for $0.5f_0 < f < 2f_0$ if $f_0 > 0.5$Hz **$_A(f) < 3$ for $0.5f_0 < f < 2f_0$ if $f_0 < 0.5$Hz**	Exceeded 0 out of 198 times	**OK**	
Criteria for a clear HVSR peak [At least 5 out of 6 should be fulfilled]			
Exists f^- in $[f_0/4, f_0]$ | $A_{H/V}(f^-) < A_0 / 2$	2.0 Hz	**OK**	
Exists f^+ in $[f_0, 4f_0]$ | $A_{H/V}(f^+) < A_0 / 2$	6.844 Hz	**OK**	
$A_0 > 2$	3.04 > 2	**OK**	
$f_{peak}[A_{H/V}(f) \pm {}_A(f)] = f_0 \pm 5\%$	|0.02067| < 0.05	**OK**	
$_f <$ (f_0)	0.08464 < 0.20469	**OK**	
$_A(f_0) <$ (f_0)	0.1224 < 1.58	**OK**	

Example 6

Class B2: strong directionality in the presence of electromagnetic disturbance, with the lack of any clear peak

Trace length: 0h20'00". Analysis performed on the entire trace.

Sampling frequency: 128 Hz

Window size: 30 s

Smoothing window: Triangular window

Smoothing: 5%

HORIZONTAL TO VERTICAL SPECTRAL RATIO

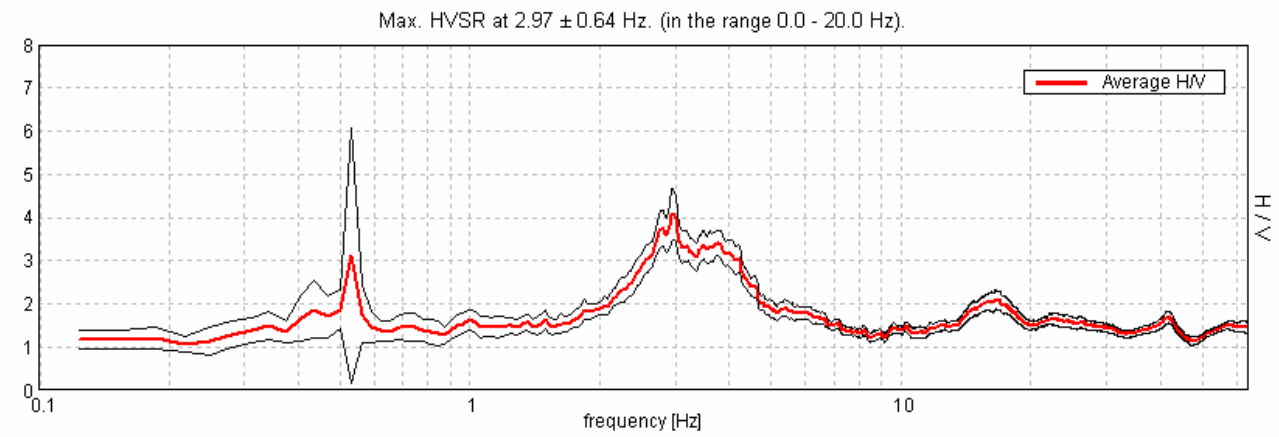

H/V TIME HISTORY

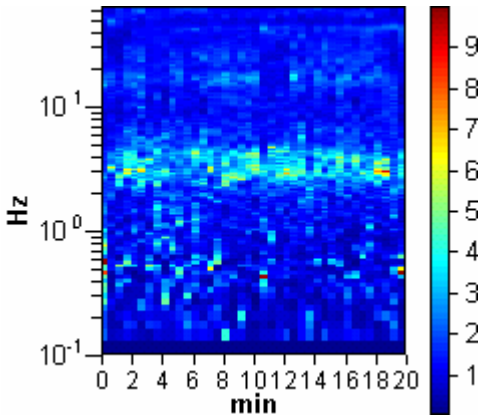

DIRECTIONAL H/V

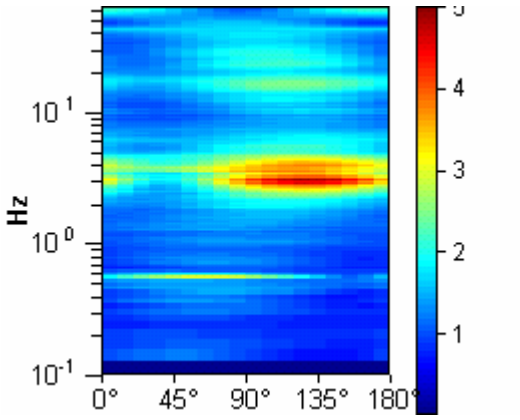

SINGLE COMPONENT SPECTRA

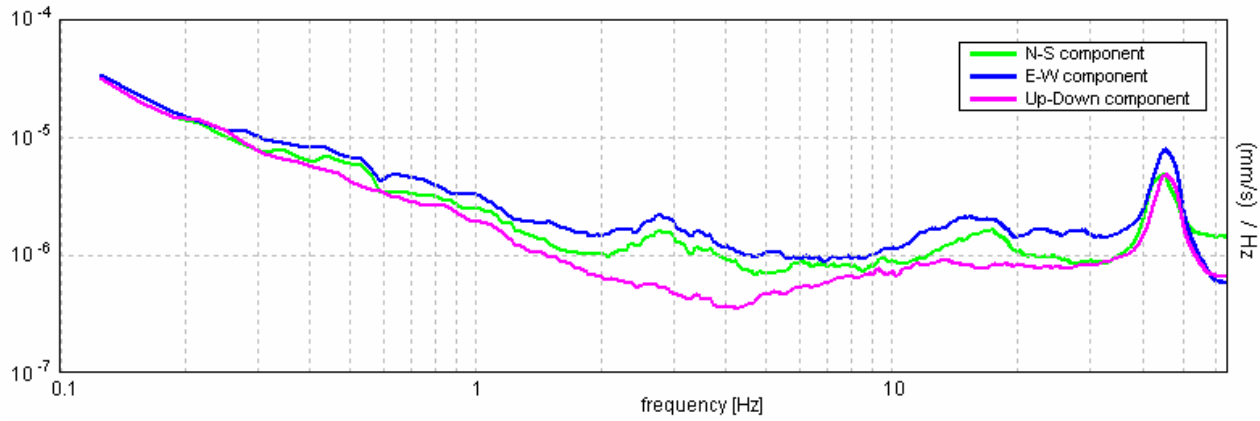

Max. HVSR at 2.97 ± 0.64 Hz. (in the range 0.0 - 20.0 Hz).

Criteria for a reliable HVSR curve [All 3 should be fulfilled]			
$f_0 > 10 / L_w$	2.97 > 0.33	OK	
$n_c(f_0) > 200$	3562.5 > 200	**OK**	
$\sigma_A(f) < 2$ for $0.5f_0 < f < 2f_0$ if $f_0 > 0.5$Hz **$\sigma_A(f) < 3$ for $0.5f_0 < f < 2f_0$ if $f_0 < 0.5$Hz**	Exceeded 0 out of 144 times	**OK**	
Criteria for a clear HVSR peak [At least 5 out of 6 should be fulfilled]			
Exists f^- in $[f_0/4, f_0]$ | $A_{H/V}(f^-) < A_0 / 2$	2.094 Hz	**OK**	
Exists f^+ in $[f_0, 4f_0]$ | $A_{H/V}(f^+) < A_0 / 2$	4.719 Hz	**OK**	
$A_0 > 2$	4.08 > 2	**OK**	
$f_{peak}[A_{H/V}(f) \pm \sigma_A(f)] = f_0 \pm 5\%$	|0.10467| < 0.05		**NO**
$\sigma_f < \varepsilon(f_0)$	0.31073 < 0.14844		**NO**
$\sigma_A(f_0) < \theta(f_0)$	0.2905 < 1.58	**OK**	